ROBUSTNESS STUDIES OF THE CMS TRACKER FOR THE LHC UPGRADE PHASE I

By

Juan Carlos Cuevas Bautista

A thesis submitted in partial fulfillment of the requirements for the degree of

MASTER OF SCIENCE

in

PHYSICS

UNIVERSITY OF PUERTO RICO
MAYAGÜEZ CAMPUS

2013

Approved by:

Héctor Méndez-Mella, Ph.D. President, Graduate Committee	Date
Samuel A. Santana-Colón, Ph.D. Member, Graduate Committee	Date
Juan Eduardo Ramírez-Vargas, Ph.D. Member, Graduate Committee	Date
Alberto Santana, Ph.D. Representative of Graduate Studies	Date
Dorial Castellanos-Rodríguez, Ph.D. Chairperson of the Department	Date

Abstract of Dissertation Presented to the Graduate School
of the University of Puerto Rico in Partial Fulfillment of the
Requirements for the Degree of Master of Science

ROBUSTNESS STUDIES OF THE CMS TRACKER FOR THE LHC UPGRADE PHASE I

By

Juan Carlos Cuevas Bautista

2013

Chair: Héctor Méndez-Mella
Major Department: Physics

Currently, several changes are being implemented in the tracker geometry of the Compact Muon Solenoid (CMS). These should improve the performance of both strip and pixel detectors. The new pixel detector will have four barrel pixel layers and three disks in the ends, compared to the current configuration of three barrel pixel layers and two disks in the ends. Also the material used to make these additional layers and disks has been reduced, yielding a lighter pixel detector and therefore, reduces the interaction of particles with the inactive material in the tracker. All these improvements are included in the CMS software (CMSSW) that simulates the response of the detector in scenarios such as increased luminosity in the Large Hadron Collider (LHC) for the period known as Phase 1 upgrade.

In this thesis, I perform some studies to show the robustness of the upgraded detector with respect to the present detector. These studies consider two scenarios with inefficiencies in the outer tracker; degradation of the first two silicon TIB layers (which are those closer to the pixel detector), and failures in some tracker modules of the outer tracker (Tracker Inner Barrel (TIB), Tracker Outer Barrel (TOB) and Tracker Inner Disk (TID)) that are believed to possibly become unstable at increasing luminosity. Finally, we study a third scenario which shows the preliminary results of a new method for simulating radiation damage on the first layer of the pixel detector.

In the first study, the degradation of the TIB is simulated due to radiation damage with a 20% uniform inefficiency in the first two TIB layers. In the second, the degradation in the outer tracker is simulated by switching off a group of selected tracker modules that could become unstable at high luminosities. Then, a new method to simulate radiation damage on the pixel detector is done through decreasing and increasing exponential functions. Next, the specifications of the new detector geometry are introduced (e.g an additional fourth barrel pixel layer) for measuring the impact of high pile-up scenarios corresponding to an increased luminosity after the Phase 1 upgrade (SLHC), thus providing feedback on the design of future CMS upgrade tracker geometries and detectors.

Resumen de Disertación Presentado a Escuela Graduada
de la Universidad de Puerto Rico como requisito parcial de los
Requerimientos para el grado de Maestría en Ciencias

ESTUDIOS DE ROBUSTEZ DEL TRAZADOR DE CMS PARA LA FASE I EN EL LHC

Por

Juan Carlos Cuevas Bautista

2013

Consejero: Héctor Méndez-Mella
Departamento: Física

En la actualidad varios cambios en la geometría del trazador del Solenoide Compacto de Muones (CMS) estan siendo implementados. Estos deben mejorar el rendimiento tanto del detector de tiras como del detector de pixeles. El detector de pixeles nuevo tendrá cuatro capas de barril de píxeles y tres discos en los extremos, en comparación con la configuración actual de tres capas de barril de píxeles y dos discos en los extremos. Además, el material empleado para hacer estas capas y discos adicionales ha sido reducido, dejando un detector de píxeles más ligero y por lo tanto, una reducción en la interacción de las partículas con el material inactivo del trazador. Todas estas mejoras son incluidas en el software de CMS (CMSSW) que simula la respuesta del detector en un escenario tal como una luminosidad aumentada en el Gran Colisionador de Hadrones (LHC) para el período de actualización conocido como Fase 1.

En esta tesis se realizan algunos estudios para demostrar la robustez del detector mejorado respecto al actual. En estos estudios se consideran dos escenarios con ineficiencias en el trazador exterior; la degradación en las dos primeras capas de silicio del TIB (son aquellas que estan más cerca al detector de pixeles) y fallas en algunos módulos del trazador exterior (TIB, TOB y TID) que se creen podrían presentar problemas al incrementarse la luminosidad. Por último, estudiamos un tercer escenario en el cual

se muestra los resultados preliminares de un nuevo método para simular el daño por radiación en la primera capa del detector de píxeles.

En el primer estudio se simula la degradación del TIB debido al daño por radiación con una ineficiencia uniforme del 20 % en las dos primeras capas del TIB. En el segundo se simula la degradación en el trazador exterior apagando un grupo de módulos seleccionados del trazador que se creen podrían dejar de funcionar a luminosidades altas. También empleamos un nuevo método para simular el daño por radiación en el detector de píxeles, con el uso de funciones exponenciales crecientes y decrecientes. Después se introducen las modificaciones de la geometría del nuevo detector (por ejemplo, una cuarta capa adicional en el barril del detector de pixeles) para medir el impacto de los escenarios con una alta cantidad de vértices primarios que se generan al incrementar la luminosidad después de la actualización (SLHC), permitiendo de esta manera optimizar el diseño de futuras actualizaciones en las geometrías del trazador y de los detectores de CMS.

This thesis is dedicated to my mom Maria Luisa Bautista, to my dad Juan Cuevas, to my sister Elba Cuevas and to my nephews Juan Esteban, Thomas and the little Sarita.

ACKNOWLEDGMENTS

"*At times our own light goes out and is rekindled by a spark from another person. Each of us has cause to think with deep gratitude of those who have lighted the flame within us*" Albert Schweitzer.

This thesis was a work of arduous research and academic preparation, many people were involved to take it to final stage, I would like to thank to these people for the support to my research and by their personal advices. These were a great light in my way, for this I want to express my sincere gratitude to:

- Dr Hector Mendez for being my guide and teach me the key particle physics concepts along my research. For his help at appropriate times and for his wise counsel on life.
- High Energy Physics group of the University of Puerto Rico, Dr Eduardo Ramirez, Dr Angel Lopez and Dr Hector Mendez for giving me the opportunity to work in the group, also for welcoming me and for their explanations of the physics involved in particle collisions.
- Dr Eric Brownson who was with me in all my work, gave me technical support and the proper advices at right time to advance in my research.
- Dr Harry Cheung for his help in my research and show me the great oportunities in the world of High Energy Physics.
- Dr Alessia Tricomi for her suggestions and questions at every tracking meeting simulation group that helped me to improved the quality of this thesis.
- My friend Cesar Pollack, he always was with me since the beginning, he taught me all his work. These were the principles of my research.
- My friend Daniel Valencia who was a personal and spiritual adviser for me. His wisdom helped me in the harder times.
- My girlfriend Nathaly for believing in me, for being my rod, to sarita for bringing sweetness to my life, both for being in my life.

- Professor Arjuna by recommend me the University of Puerto Rico and for his valuable advices to triumph in physics and the life.
- And for all my old friends in Colombia and my new friends in Chicago and Puerto Rico, Sergio I, Deisy, Amanda, Jose Luis, Ruth, Indira, Izamar, Jose, David, Carlos, Soraya, Yamile, Maria, Hector, Sergio II and more, they were with me along the road that finally led me to finish my research.

TABLE OF CONTENTS

LIST OF TABLES

LIST OF FIGURES

CHAPTER 1
LARGE HADRON COLLIDER (LHC)

1.1 What is it?

The European Organization for Nuclear Research (CERN) is a complex of many accelerators, that is mainly constituted of a 27 km ring in circumference of superconducting magnets with circular structures to boost the energy of the particles along the beam pipe (Figure 1–1).

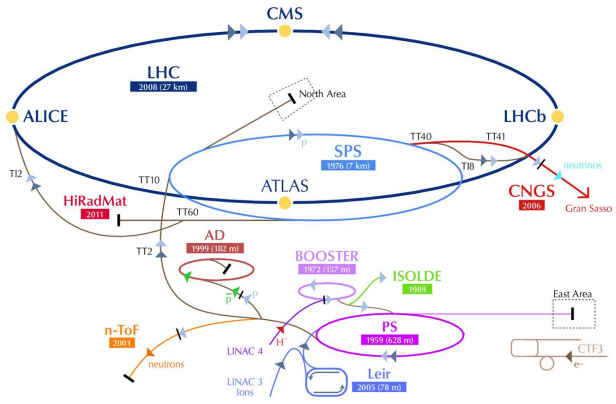

Figure 1–1: CERN complex [2].

Two beams made of bunches of charged particles travel with high velocities close to the speed of light in opposite ways in separate beam pipes. They are driven around the accelerator ring by thousands of magnets that produce a strong magnetic field (8T), in order to keep the circular path of the bunches and make them collide at the interaction point (Figure 1–2).

The Large Hadron Collider (LHC) at CERN is the biggest particle accelerator in the world. The beams inside the LHC are made to collide at four points around the accelerator ring, corresponding to the positions of particle detectors [2].

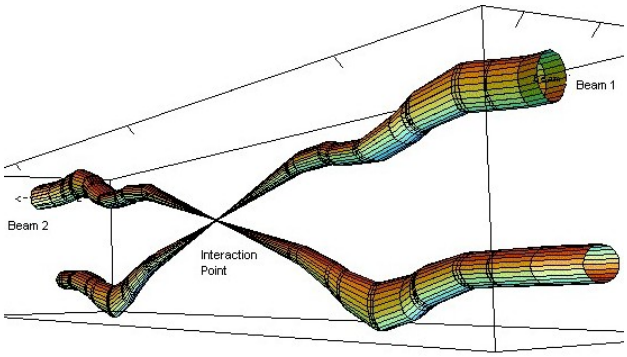

Figure 1–2: Interaction point: the spot where the particle beams collide [3].

As shown in Figure 1–1, before the particle beam enters into the LHC, it passes through a series of rings to be accelerated up:

- Hydrogen atoms are taken from a bottle containing H_2. The protons are extracted from hydrogen atoms.
- The protons are injected into the PS Booster (PSB) from the Linear Accelerator (LINAC2) with a speed near to $0.3c$ (it means 0.3 times the speed of light).
- The booster accelerates them to 0.87 times the speed of light, then passing through to Proton Synchrotron (PS) and then to Super Proton Synchrotron (SPS), where they are accelerated to be transferred to the LHC (one in clockwise and the other a counterclockwise direction).
- Finally, in the LHC they will be accelerated for around 20 minutes. In normal operating conditions the beams will be circulating for many hours inside the LHC beam pipes [14].

1.1.1 Description of the Large Hadron Collider

As mentioned previously, the particles are accelerated through different boosters and simultaneously their energy increases each time they are accelerated. The LHC was built in this manner because it takes advantage of the directions in which the beams travel. When two beams traveling in opposite directions, the energy of the collision is the sum of the energies of the beams collide, while a beam with the same energy that hits

a fixed target would produce a collision with less energy [15]. The particles accelerated in the LHC need to have electric charge to be directed by the magnetic field, thus the particles that can be accelerated are protons and ions.

The LHC was designed with specific characteristics for detecting and studying different kinds of particles, some important definitions used commonly in the studies made in the detector are:

- **Instantaneous Luminosity ($\mathscr{L}$)**: it is a measurement of the number of collisions that can be produced in a detector per cm^2 and per second,

$$\mathscr{L} = \frac{NN}{tS_{eff}}$$

where N is the number of protons because each particle in a bunch might collide with any other from the bunch approaching head on, t is the time between bunches and S_{eff} is the section effective of collision.

From the experimental data

$$N^2 = (1.15 \times 10^{11})^2,$$
$$t = 25 \times 10^{-9} s,$$
$$S_{eff} = 4\pi(16 \times 10^{-4})^2 cm^2$$

substituting

$$\mathscr{L} = 10^{34} cm^{-2} s^{-1}.$$

Initially the LHC was conceived to run at a peak instantenous luminosity of $\mathscr{L} = 10^{34} cm^{-2} s^{-1}$, but currently an upgrade is being planned for 2013 to double the luminosity.

- **Cross section $\boldsymbol{\sigma}$** is a measurement of the probability that an event (collision at the interaction point) occurs. It is measured in barns $1b = 10^{-24} cm^2$.

- **Pile Up** are the additional interactions that will be superimposed to the observed event, causing multiple events in the same time gate as the event of interest [3].

The study of the interactions carried out in the LHC will improve our current understanding of the universe. So far the most successfully theory in explaining the fundamental forces is the Standard Model (see section 1.3), but it still has many questions that need to be answered. For this purpose, the LHC has various experiments which main goals are:

1. Explain the origin of mass, why some particles are very heavy while others have no mass at all. The proposed explanation is called Higgs mechanism, the whole space is filled with a 'Higgs field', and by interacting with this field, particles acquire their masses. The Higgs field has at least one new particle associated with it, the Higgs boson. The recent discovery of the Higgs Bosson announced on July 4, 2012 in CERN has turned the LHC efforts in studying whether the observed couplings of the new particle to other fundamental particles match the predictions for a SM Higgs boson. So far, only there are a few channels of production mechanism for the Higgs boson well studied [16, 17].
2. The Standard Model does not offer an unified theory that can explain the four fundamental forces satisfactorily. The principal issue is constructing a theory that joins gravity with the other fundamental forces. Actually Supersymmetry (SUSY) is a theory that assumes the existence of more massive partners of the particles of the standard model [14]. The observations conducted by the LHC to date, don't show new physics in this domain with 95% confidence levels [18].
3. The Standard Model can explain the beginning of the universe seconds after the big bang. The studies of proton-proton collisions at the LHC will provide a clue of the state of matter that would have existed in the early universe, called "quark-gluon plasma".

These studies are carried out by six experiments at the LHC, two large multipurpose experiments (study various topics mentioned previously) ATLAS and CMS detectors. Two medium-size experiments ALICE and LHCb have specialized detectors for analyzing the LHC collisions in relation to specific phenomena. Two experiments, TOTEM and LHCf, designed to focus on forward particles (protons or heavy ions). The principal goals of each of these experiments are [19]:

- **ALICE**: A Large Ion Collider Experiment. It studies a state of the matter known as quark-gluon plasma, which is believed to have existed just after the Big Bang.
- **ATLAS**: study of the different Higgs boson production mechanisms and search for it, extra dimensions, and particles that could make up dark matter.
- **CMS**: it has the same scientific goals than ATLAS experiment, but it has a different detector to achieve these purposes.
- **LHCb**: Large Hadron Collider beauty. It specialises in investigating the slight differences between matter and antimatter by studying a type of particle called the beauty quark.

For physicists, the most important parameters are the beam energy and the number of interesting events that can be produced in the particles' collision at high energies.

Once the scientists have gathered all information, they have to analyze it. For each collision it must count, track and characterize all the different particles that were produced in order to reconstruct the kinematic of the physical process. The track of the particle brings back much useful information. For instance if the orientation of the magnetic field is known, trough the deflected way of the particle, the charge of the particle can be inferred, this being negative or positive. Also the momentum of the particle can be computed: particles with a high momentum ($\sim$0.6 GeV) will remain with an undeflected trajectory, while the particles with low momentum will ($\sim$0.2 GeV) make tight spirals.

The LHC has various experiments for measuring the position in space, the momentum, the mass and the energy of the particles. The particles will travel through different sub-detectors or layers, depending of their charge these could be separated and allow thus the measurement of their momentum. The current detectors do not make the tracks directly, instead, they produce electrical signals that can be recorded as computer data. A specialized software reconstructs the pattern of tracks recorded. The LHC will deliver data around 40 million times per second, and there will only be 100 collisions of interest per second. These collisions are directly linked with the decays of or toward 'Higgs' bosson. Only a few collisions could help to the discovery of 'Higgs' bosson and therefore to the validation of the Standard Model.

1.2 Super Large Hadron Collider (SLHC)

The SLHC is a proposal to extend the physics tools of the LHC with an increase in the luminosity. The aim is to increase the luminosity by a factor of ten. The upgrades are needed because of degradation of the detectors in the LHC caused by the increase of the radiation.

Some of these upgrade characteristics are: extending the mass reach and improve the precision to measure the parameters for new physics. With these conditions it is expected to discover physics beyond the SM. Two scenarios were considered, the first phase would aim to carry an instataneous luminosity of 2×10^{34} $cm^{-2}s^{-1}$ through of replacement of the inner triplet focusing magnets [20]. The second phase will reach 10^{35} $cm^{-2}s^{-1}$. In this scenario a bunch of either 25 nd or 25 ns will be included. This will require of the positioning of dipole magnets closer to the interaction point, thus improving the beam focusing, based on early separation of proton beams.

1.2.1 Upgrade of the CMS and ATLAS detectors for the SLHC

To bear the high luminosity conditions in the SLHC the Multipurpose experiments will make some upgrades. The most significant upgrade for both ATLAS and CMS

will be the replacement of the inner tracker system. The new trackers will have also to be redesigned to handle pattern recognition performance. In general, all aspects of an experiment need to be considered: detectors, electronics, powering, cooling, readout, etc. The hadronic calorimeter scintillator may suffer radiation damage in the forward regions. This will mean using more detector channels to keep pattern recognition performance. Because of radiation damage and increasing particle occupancies CMS will require new inner tracks. Currently various studies are being carried out for looking the impact on detectors, electronics, engineering, readout, powering, cooling, data-acquisition, trigger and computing [20].

1.3 Standard Model

The functioning of the universe can be explained with the fundamental interactions between the elements that constitute it. These interactions are the fundamental forces; a fundamental force is one that does not arise from another basic force. Particle physics tries to explain all interactions within an unified framework (Figure 1–3).

The standard model recognizes four forces as being sufficiently distinct and elemental to be called fundamental forces (the Gravitational Force is not part of Standard Model, and since no quantum gravity found yet) [21]:

1. **Gravitational Force:** is the most common of the four forces. It is present in all phenomena of our daily life, for instance it makes the objects fall to the ground, it binds matter in planets and stars and holds stars together in galaxies and it is responsible for the motion of the earth around the sun. However its effective strength is smallest compared with the other forces for microscopic distances.
2. **Electromagnetic Force:** this force can be attractive or repulsive as opposed to the gravitational force, which is only attractive. It acts on charged particles, hence it is responsible for binding atoms into molecules.

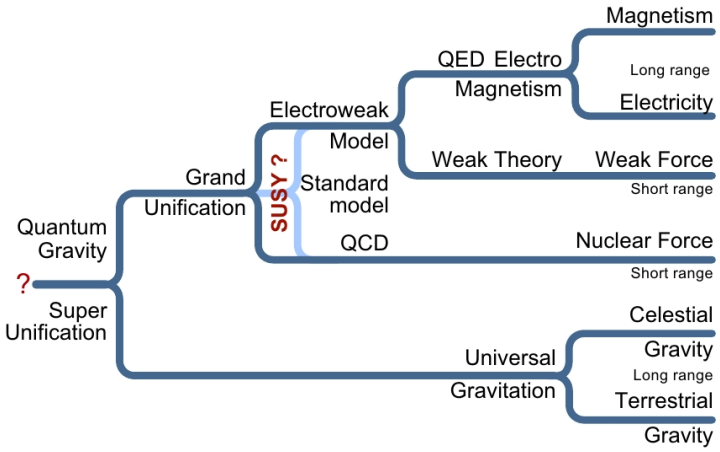

Figure 1–3: Theories of Unification [4].

3. **Weak Force:** is responsible of the decays of particles and nuclei (beta decay, etc) as well as in the interactions of neutrinos. For instance in nuclear reactions in the center of the sun, where hydrogen is converted into helium. The weak force is a complex theory because it lets particles change from one type to another. The weak force explains the generation structure of the quarks and leptons, if two leptons are interacting within range of the weak force, it is possible for them to be changed into other leptons within the same generation (see Figure 1–4). Similarly the weak force can turn one quark into another and again the force acts within the generations of quarks. The weak force can act within the lepton and quark generations, but not between them.

4. **Strong Force:** is responsible for holding together quarks to make protons and neutrons (and other particles). Only the quarks can feel the strong force and hence the division of the material particles into the quarks and leptons. Current theories of the strong force suggest that it is impossible to have a single isolated quark without any other quarks, this theory is called theory of quark confinement. When a new quark is created in the experiments, they rapidly combine with others, this makes it very difficult to study [21].

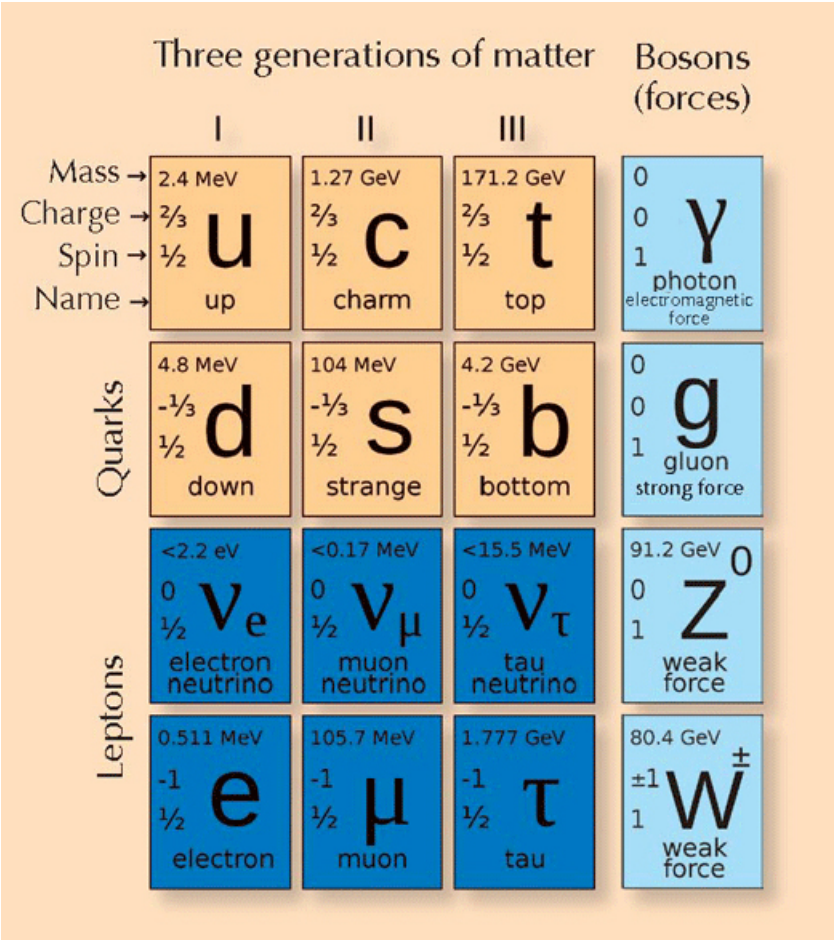

Figure 1–4: Constituents of Matter [5].

Figure 1–4 summarizes briefly the principal interactions and its mediators. The generations in the table are labeled by columns, being I the first generation and so on consecutively. The first quantity in the cell is the mass of the particle in electron-volts over the speed of light squared (eV/c^2)(an electron-volt is the amount of energy gained or lost by an electron traversing an electric potential difference of one volt), the second is the charge in elementary charge units (e), and the third is the spin in natural units ($\hbar$) with the name of the particle below of its respective symbol. For instance, the up quark has a mass of 2.4 MeV/c^2, a charge of 2/3 and a spin of 1/2 and it is represented by the letter **u**. The quarks occupy the upper cells of the table and the leptons occupy

the lower cells.

The *Standard Model* joins three of the four fundamental forces (electromagnetic, weak, strong) previously explained, it explains the structure of the matter and how the fundamental particles interact between them (Figure 1–3). The fundamental particles (they are not composed of any other particle) are twelve, these are divided into two distinct groups called the quarks and leptons. There are six flavors or quarks called up (u), down (d), strange (s), charm (c), bottom (b) and top (t). The six leptons are the electron (e), electron-neutrino (ν_e), the muon (μ), muon-neutrino (ν_μ), tau (τ) and tau-neutrino (ν_τ) (see Figure 1–4). Their position on the table depend of the mass, each member of a family or generation has greater mass than the corresponding particles of lower generations. A particle with a big mass needs more energy for being produced in the laboratory, formerly the accelerators had not enough energy for producing these particles.

The electron, the muon and the tau, have all the same electrical charge and interact with the same fundamental forces, however their masses are different and the only stable (the stable term makes reference to the lifetime of the particles, the proton being the most stable particle of the standard model) is the electron. The tau and muon can decay into other particles. Each one of these leptons have their respective neutrino, they are electrically neutral and have smaller masses. Experiments with the electron-neutrino suggest that its mass is less than one ten-thousand of the electron [21]. Leptons feel all forces except for the strong force, for this reason can be found isolated in universe. On the other hand the quarks feel the strong force, this force holds them together to form more particles such as the hadrons (baryons and mesons). (See Table 1–1)

Table 1–1: Baryonic Octet.

Baryon Octet			
qqq	Q	S	$Baryon$
uud	1	0	p
uus	1	-1	Σ^+
udd	0	0	n
uds	0	-1	Σ^0
uds	0	-1	Λ
uss	0	-2	Ξ^0
dds	-1	-1	Σ^-
dss	-1	-2	Ξ^-
udc	1	0	Λ_c^+

Three quarks in a bound state conform a baryon. A quark and an antiquark conform a meson. They can be sorted out according to their quantum numbers, the baryon number B, strangeness, charmness, upness, bottomness, downness, topness and their electric charge Q. A baryon has $B = 1$ and an antibaryon has $B = -1$, the charge vary according to quark composition, the quarks has fractionary charges and the sum of all charges of each quark gives the charge of the hadron. The hadrons are particles which experience the weak and strong interaction and, the charged ones, electromagnetic interactions. The last column in the Figure 1–4 indicates the type of interaction in which leptons and quarks participate, each of them is mediated by the exchange of vector bosons: electromagnetic (γ photon), strong (gluon **g**) and weak (**z** y $w^{\pm}$). Gluons carry color charge, bosons carry weak charge and couple with each other as well [22].

1.3.1 Beyond the Standard Model

Although the Standard Model is one of the most successful theories of particle physics, there are still some theoreticall problems that it has not been able to explain [23]. Two of the principal theories that attempt to solve some inconsistencies not resolved yet by the Standard Model, and are the subject of extensive research at the LHC:

- **Supersymmetry (SUSY):** so far, one of the big challenges of particle physics is to link gravity with the three remaining fundamental forces. One theory that could provide

a solution in this issue would be the SUSY. It attempts to establish a relationship between matter particles (fermions) and the force carriers (bosons) that would allow them become from one type of particle to another with no distinction. According to the theory, each of the fundamental particles would have a supersymmetric partner (sparticle). For instance, the supersymmetric partner of the gluon would be the gluino and the squark for the quark. The decays of SUSY particles, such as squarks and gluinos involve cascades that always contain the lightest SUSY particle (LSP). If the SUSY particle interact very weakly, it will lead a significant missing transverse energy (E_T^{miss}) in the final state [18].

- **Extra Dimensions:** in search for a unified theory in which gravity can be included with the other three fundamental forces, it is proposed the existence of extra dimensions to the four already known (one of time and three spatial). It is assumed that these dimensions are so compressed (with radii much larger than the Planck length ($10^{-35}m$) although smaller than $10^{-18}m$) that we can not measure them directly. Their observation could lead to a consistent framework as mathematically as experimentally [19].

CHAPTER 2
THE COMPACT MUON SOLENOID DETECTOR

The Compact Muon Solenoid (CMS) detector is a multi-purpose apparatus designed to operate at the Large Hadron Collider (LHC) at CERN. The CMS detector was designed to explore the physics phenomenas presented by the LHC. Some of the studies carried out by the CMS are:

- **The Higgs Boson Status**: as it was described in the previous chapter, the Standard Model explains natural phenomena in term of the interactions between fundamental particles like quarks and leptons through of the exchange of force carriers like bosons. However the question of how particles acquire mass is still a mystery. To resolve this question the Standard Model predicts the existence of the Higgs boson (H), a scalar particle associated with the field responsible for spontaneous electroweak symmetry breaking. The discovery of the Higgs boson with an approximately mass of 125 GeV in the Large Hadron Collider (LHC) was reported on July 4 2012 by ATLAS and CMS simultaneously. "The observation of a Higgs boson with a mass of 125 GeV is consistent with the theoretical constraint coming from the unitarization of diboson scattering at high energies. However, there is still a possibility that the newly discovered particle has no connection to the electroweak symmetry breaking mechanism. In addition, several popular scenarios, such as general two-Higgs-doublet models or models in which the SM Higgs boson mixes with a heavy electroweak singlet, predict the existence of additional resonances at high mass, with couplings similar to the SM Higgs boson. In any such models, issues related to the width of the resonance and its interference with non-resonant WW and ZZ backgrounds must be understood" [24].
- **Search for supersymmetric particles (SUSY particles)**: CMS search the sparticles through different mechanisms: collecting and adding up the momenta and energies

of all the emerging particles from a collision (momentum conservation). If the final momentum seem different from the initial momentum, it is possible that a LSP has been produced, and it has the difference in the momentum. For this reason CMS is so hermetic as possible. To provide good containment of particles for the measurement E_T^{miss}, CMS is equipped with the Hadron Calorimeters (HCAL). These are placed in the forward region, at angles almost parallel to the beam tube, in this manner the particles scattered in all directions can be detected. In SUSY events the final decay products will often consist of pairs of leptons of opposite charge (e.g. a muon and an anti-muon), along with the ever present LSPs. High levels of pairs of these particles should be a clear signal of SUSY. With this purpose CMS has placed an accurate Electromagnetic Calorimeters (ECALs) and Muons detectors on its ends [18].

- **Search for Extra dimensions**: *theories that postulate these extra dimensions predict that, like an atom having a low energy ground state and then more energetic states, there must be heavier versions of standard particles recurring at higher and higher energies as they navigate smaller dimensions* [4]. Finding fundamentals particles such as W and Z in CMS at low energies could confirm the existence of extra dimensions [19].
- **Heavy-ion physics**: Recent studies from RHIC indicate that very strongly interacting nuclear matter is produced in high energy heavy-ion collisions [25]. At high enough energies the relevant degrees of freedom are expected to be quarks and gluons rather than hadrons, forming the quark gluon plasma. The increase in collision energy from $\sqrt{s_{NN}} = 200$ GeV/c^2 at RHIC to 5500 GeV/c^2 at LHC will allow studies of presently inaccessible hard probes like Υ and Z^0 [25].

The technical requirements for CMS to achieve the goals of the LHC physics challenges can be summarized as follows [26]:

- Good charged particle momentum resolution and reconstruction efficiency in the inner tracker.
- Good E_T^{miss} and dijet mass resolution, requiring hadron calorimeters with a large hermetic geometry coverage.
- Good electromagnetic energy resolution, good diphoton an dielectron mass resolution ($\approx 1\%$ at 100 GeV/c^2), measurement of the direction of photons and/ or correct localization of the primary interaction vertex, π^0 rejection and efficient photon and lepton isolation at high luminosities.
- Good muon identification and momentum resolution, good dimuon mass resolution ($\approx 1\%$ at 100 GeV/c^2) and the ability to determine unambiguously the charge of muon with $p < 1$ TeV/c.

2.1 How does the CMS work?

2.1.1 Generalities

Modern particle detectors consist of layers of sub-detectors, each one with a specific function and therefore specialized in a kind of particle or property. The main function of a particle detector is to record and visualize the events that result from the collision at the accelerator. The information obtained on a particle's momentum, energy, and charge, helps identify the particle that has passed through a detector. There are 2 main types of subdetector (Figure 2–1):

- **Tracking chamber:** this region is the inner part of the detector, it is filled with highly segmented sensing devices of various kinds. It can detect and reveal the paths of electrically charged particles through the interaction of them with the atoms of the substance that make up the detector, so they leave behind samples of energy that become tiny electrical signals that can be stored as computer data. This data can be used to reconstruct the pattern of tracks left by the particles. For instance with the curvature of a particle's track and the value of the magnetic field, the momentum of a

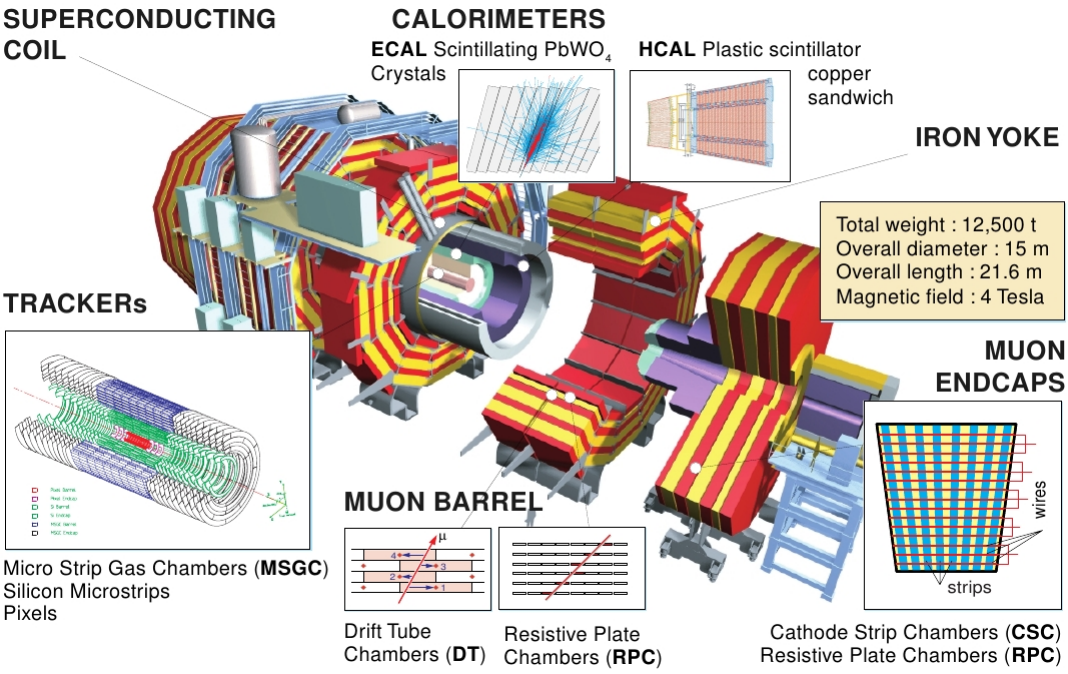

Figure 2–1: Overall layout of CMS detector [4].

particle is measured. Muon chambers are tracking devices used to detect muons. These particles interact very little with matter and only muons and neutrinos can travel long distances through dense material. Usually the muon chambers are situated in the outer layers of the detector, and once there, the neutrinos are detected like residual energy or "missing energy" [15].

- **Calorimeters:** A calorimeter is designed to stop or absorb most of the particles coming out of collisions, this way it can measure the energy deposited by the particles within the detector. Generally it is made out of layers of passive or absorbing high density material interleaved with layers of active medium such as solid lead-glass or liquid argon. In the CMS detector there are two types of calorimeters:
  - **Electromagnetic Calorimeter (ECAL):** it measures the total energy of light particles such as electrons e^-, positrons e^+ and photons γ. These particles produce electromagnetic showers of e^-/e^+ pairs in the material. The electrons or positrons

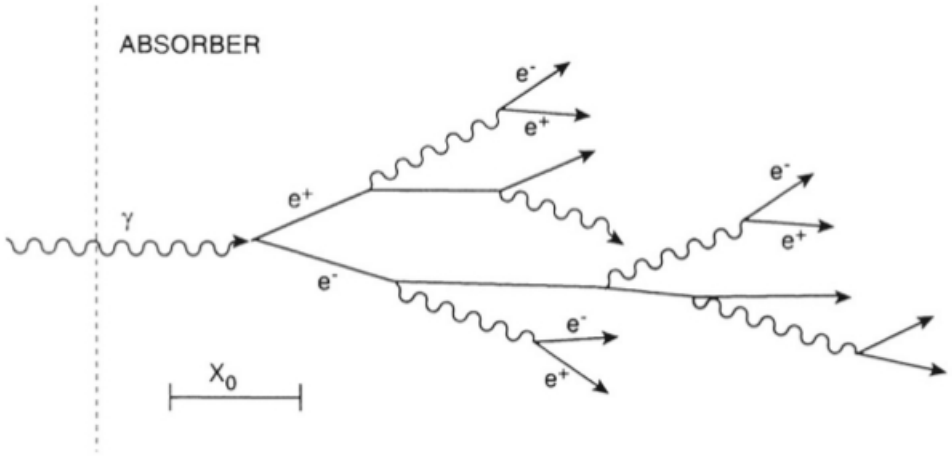

Figure 2–2: Electromagnetic shower [6].

are deflected by the electric field of atoms, causing them to radiate photons. The photons then make e^-/e^+ pairs, which then radiate more photons. The number of final electron-positron pairs is proportional to the energy of the incident particle (Figure 2–2).

– **Hadron Calorimeter (HCAL):** it measures the total energy of hadrons. They interact with the dense material that make up the detector producing a shower (Figure 2–3).

2.1.2 The CMS detector in action

The global coordinate system adopted by CMS is in terms of cylindrical coordinates (Figure 2–4). The origin is centered at the nominal collision point (where the protons collide) inside the experiment, the y-axis pointing vertically upward, the x-axis pointing radially inward toward the center of the LHC and the z-axis points along the beam line (the path that protons travel in opposite directions). The azimuthal angle ϕ is measured from the x-axis in the x-y plane and the radial coordinate in this plane is denoted by r. The polar angle θ is measured from the z-axis. The transverse momentum P_T is used to describe the kinematics of produced particles along the proton direction, this

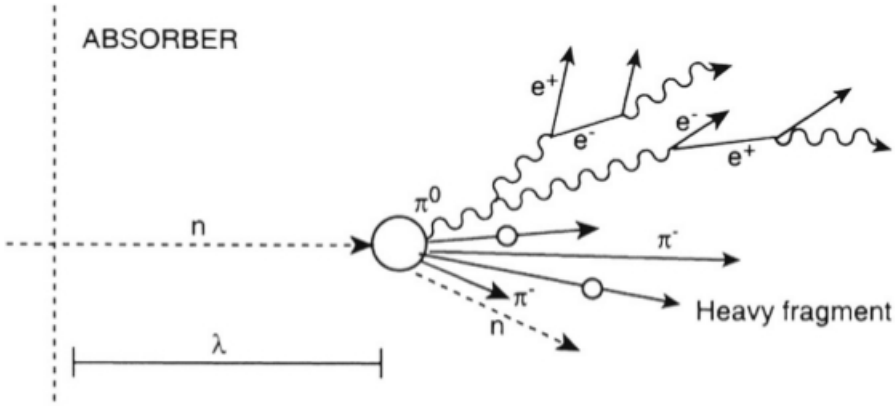

Figure 2–3: Hadronic shower: the upper part of the diagram is the electromagnetic component and the lower part is the hadronic component [6].

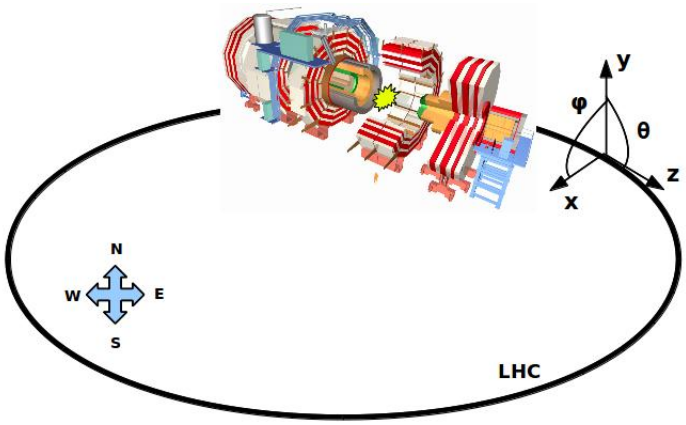

Figure 2–4: CMS global coordinate system with respect to the LHC.

is the momentum component in x-y plane. Also the angle between the z-axis and the momentum vector (θ), the angle between the P_T vector and the x-axis (ϕ) and the longitudinal momentum P_z are used (Figure 2–5). The rapidity (y) is a Lorentz boost variable for this reason the physics prefers the pseudorapidity variable for describing the kinematic of the particles. The rapidity is a dimensionless quantity that gives us information about the energy E and the longitudinal momentum P_z of the particle. Energy and momentum are quantities that can be measured in the subdetectors, the

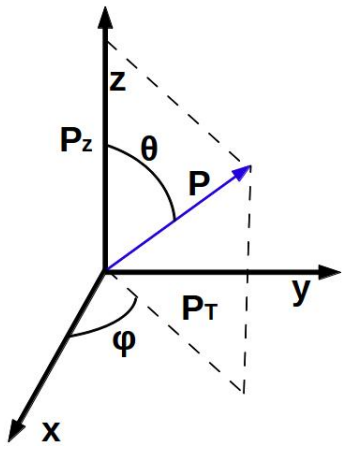

Figure 2–5: Vector momentum P with respect to cilindrical coordinates. P_T is the transverse momentum to beam line, θ is the polar angle, ϕ is the azimutal angle and P_z is the longitudinal momentum [6].

rapidity depends on the frame of reference and is related to rapidity in another frame by an additive constant. It is defined as follows

$$y = \frac{1}{2} \ln \left(\frac{E + p_z}{E - p_z} \right) \tag{2.1}$$

Usually in the experiments it is only possible and easier to measure the angle of the detected particle relative to the beam line (Figure 2–6). In that case it is convenient to utilize this information by using the *pseudorapidity* (η) to characterize the detected particle.

The pseudorapidity is an approximation of the rapidity in the case that the transverse momentum of the particle is much greater than its rest mass and this particle moves with a speed close to the speed of light [27]. With these assumptions the pseudorapidity is:

$$\eta = - \ln \left[\tan \left(\frac{\theta}{2} \right) \right] \tag{2.2}$$

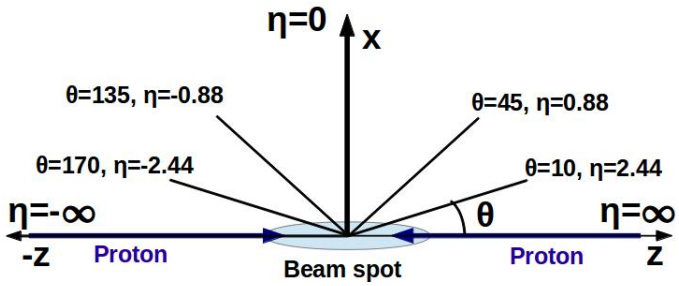

Figure 2–6: Pseudorapidity values for the principal polar angles.

The CMS detector is 21.6 m long and has a diameter of 14.6 m, its total weigh is 12500 tons. Its principal characteristic is a huge, high magnetic field (4 Tesla) solenoid, 13 m in length and 6 m in diameter. It was designed in such manner that it contains the electromagnetic and hadron calorimetry surrounding a tracking system and allows an accurate detection of muons. When the bunches of protons collide at the interaction point, the magnetic field produced by the solenoid will bend the paths of particles emerging from the collision. The particles with a larger momentum will have a path almost as a straight line and the particles with less momentum will bend its path forming a curve. This path will be useful for measuring the charge-mass ratio and the momentum of particles (Figure 2–7).

The muon path (blue line) traverses the whole detector despite the magnetic field, because of its little interaction with the matter and high momentum, while the charged particles (green and red line) are stopped at the first layer of the detector (ECAL). Finally the neutral particles path (green and blue dashed lines) like the neutron and photon remain undeflected and they are stopped by the HCAL and ECAL respectively (Table 2–1).

2.1.3 The subdetectors in CMS

In the CMS detector there are four muon stations (Figure 2–1). Each muon station consist of several layers of aluminium drift tubes (DT) in the barrel region and cathode

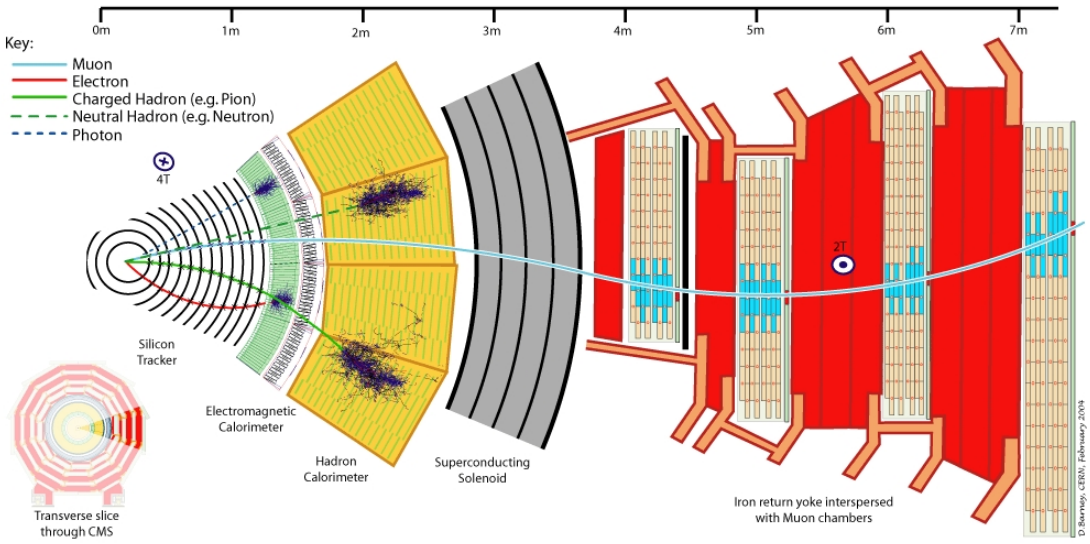

Figure 2–7: (Transverse slice through CMS). Detection of the particles coming out of a collision by CMS detector [2].

strip chambers (CSC) in the endcap region and it is complemented by resistive plate chambers (RPC) in the barrel and endcap region [7].

The electromagnetic calorimeter (ECAL) uses lead tungstate ($PbWO_4$) crystals with coverage in pseudorapidity up to $|\eta| < 3.0$ to measure the energy of charged interacting particles, like electrons and photons. The $PbWO_4$ as scintillation crystal has the advantage of a fast response time and high radiation resistance. The scintillation light produced in the crystals is detected by silicon avalanche photodiodes (APDs) in the barrel region and by vacuum phototriodes (VPTs) in the endcap region. A preshower system is installed in front of the endcaps to keep a reliable isolation of single photons and photons produced in pairs in neutral pion decays [7].

The ECAL is surrounded by a brass/scintillator sampling hadron calorimeter (HCAL) with coverage up to $|\eta| < 3.0$. The HCAL is a sampling calorimeter built from alternating layers of massive absorbing brass plates and plastic scintillator tiles arranged in trays. The plastic scintillator tiles are read out by wavelength shifting fibers that shift

Table 2–1: What we see in the CMS subdetectors [1].

$Leptons$	$Vertexing$	$Tracking$	$ECAL$	$HCAL$	$MuonCham.$
$e^{\pm}$	$\times$	$\overrightarrow{P}$	E	$\times$	$\times$
$\mu^{\pm}$	$\times$	$\overrightarrow{P}$	✓	✓	$\overrightarrow{P}$
$\tau^{\pm}$	✓$\times$	✓	$e^{\pm}$	$h^{\pm}, 3h^{\pm}$	$\mu^{\pm}$
ν_e, ν_μ, ν_τ	$\times$	$\times$	$\times$	$\times$	$\times$
$Quarks$					
u, d, s	$\times$	✓	✓	✓	$\times$
$c \longrightarrow D$	✓	✓	$e^{\pm}$	h, S	$\mu^{\pm}$
$b \longrightarrow B$	✓	✓	$e^{\pm}$	h, S	$\mu^{\pm}$
$t \longrightarrow bW^{\pm}$	b	✓	$e^{\pm}$	$b + 2 \quad jets$	$\mu^{\pm}$
$Gauge \quad Bosons$					
γ	$\times$	$\times$	E	$\times$	$\times$
g	$\times$	✓	✓	✓	$\times$
$W^{\pm} \longrightarrow l^{\pm}\nu$	$\times$	$\overrightarrow{P}$	$e^{\pm}$	$\times$	$\mu\pm$
$W^{\pm} \longrightarrow q\bar{q}$	$\times$	✓	✓	$2jets$	$\times$
$Z^0 \longrightarrow l^+l^-$	$\times$	$\overrightarrow{P}$	$e^{\pm}$	$\times$	$\mu^{\pm}$
$Z^0 \longrightarrow q\bar{q}$	$(b\bar{b})$	✓	✓	$2jets$	$\times$

the blue-violet light emitted by the scintillator to green light which is then sent through transparent fibers to hybrid photodetectors (HPDs) with 19 independent pixels [7]. The first scintillators are placed in front of the first absorber plate in order to sample showers developing in the material between the ECAL and the HCAL, while the last scintillators are installed after the last absorber plate to correct for late developing showers leaking out. This central calorimetry is complemented by a *tail-catcher* in the barrel region (HO) ensuring that hadronic showers are sampled with nearly 11 hadronic interaction lengths. Coverage up to a pseudorapidity of 5.0 is provided by an iron/quartz-fiber calorimeter used as active medium. A longitudinal fragmentation in two parts allows to distinguish signals generated by electrons and photons from signals generated by hadrons [7].

2.2 CMS Tracking chamber

The CMS tracking chamber was designed to provide an accurate and efficient measurement of tracks of the charged particles coming out from the LHC collision and a precise reconstruction of primaries and secondaries vertices. It is the central part of the

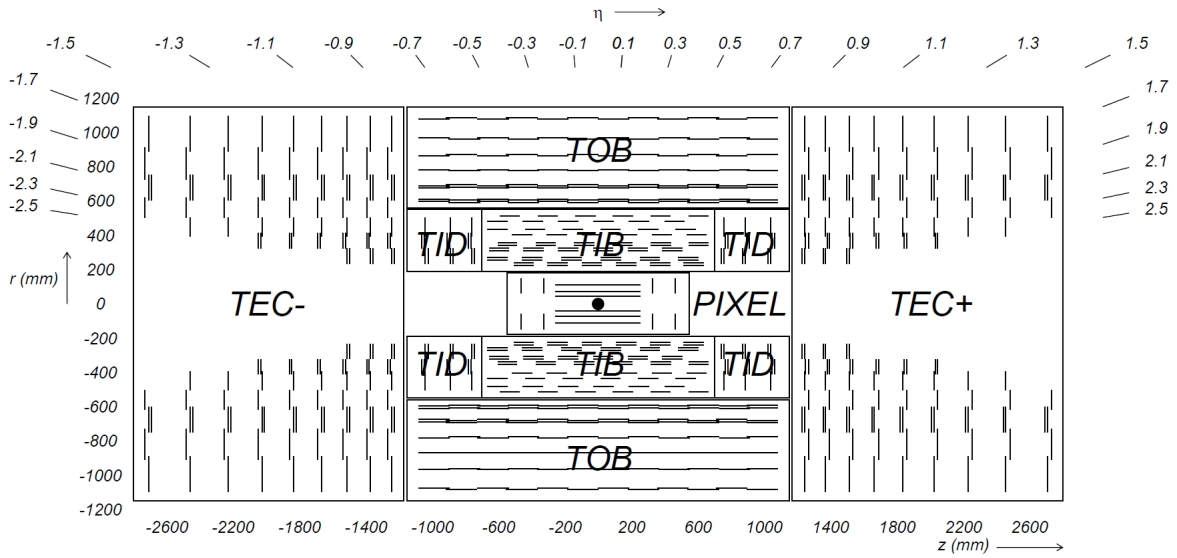

Figure 2–8: Side view of the CMS tracker. Each line represents a detector module. Double lines indicate back-to-back modules which deliver stereo hits [7].

detector (Figure 2–1), it has a length of 5.8 m and a diameter of 2.5 m. At the LHC design luminosity of $10^{34} cm^{-2} s^{-1}$ there will be on average about 1000 particles from more than 20 overlapping proton-proton collisions traversing the tracker for each bunch crossing [26]. It is expected that the detector can keep a minimum amount of material in order to limit multiple scattering, bremsstrahlung, photon conversion and nuclear interactions. All these difficulties mean that the detector should have a big granularity and fast response in such manner that the trajectories can be identified reliably. To optimize the reconstruction of trajectories, the tracking chamber (Figure 2–8) is composed of a pixel detector and the Silicon Strip Tracker [7].

2.2.1 Pixel Detector

The pixel detector consists of three barrel layers (BPIX) at radii between 4.4 cm, 7.3 cm and 10.2 cm, it extends along z with a length of 53 cm. In addition it has two

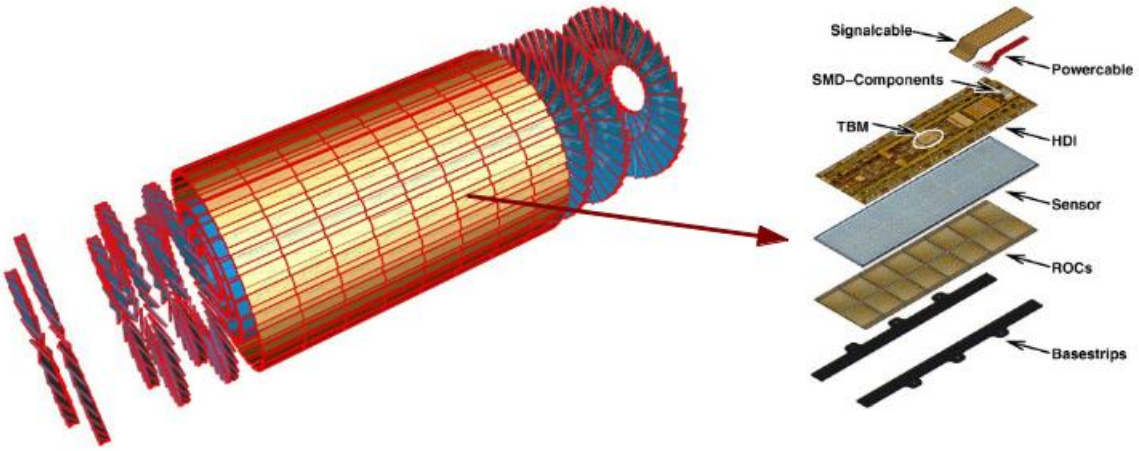

Figure 2–9: An exploded view of CMS Pixel Detector and a barrel pixel module [8].

disks of pixel modules on each side (FPIX) extending from 6 to 15 cm in radius. Each pixel module consisting of thin, segmented n-on-n silicon sensors with highly integrated readout chips (ROC) connected by indium bump-bonds (Figure 2–9). The pixel sensor modules were designed and arranged in the CMS tracker in such manner, that they can provide three accurate space points in $r - \phi$ and z of each charged particle trajectory [8]. The pixel detector covers a pseudorapidity range $-2.5 < \eta < 2.5$, matching the acceptance of the central tracker. It is essential for the reconstruction of secondary vertices from b and tau decays, forming seed (see Chapter 4) tracks for the outer track reconstruction and high level triggering (this computerized system choose the interesting events that could involve a Higgs boson decaying) [7].

2.2.2 Silicon Strip Tracker

The Silicon Strip Tracker occupies the most inner region of CMS. It is composed of several cylindrical concentric layers extending from 0.2 m to a radius of 1.1 m and has a length of 5.6 m along the beam pipe direction. These cylindrical structures are what make up the Tracker Inner Barrel (TIB) and the Tracker Outer Barrel (TOB). The TIB

has four barrel layers assembled in shells; the two innermost layers host double-sided detectors glued back to back to provide an accurate measurement of the $r - \phi$ and z coordinates of charged particles. Three small disks (TIB) at each end of the TIB provides a full coverage. The TOB consists of six concentric layers, also with double-sided modules in the two innermost layers and 9 disks (TEC) on both side of the barrel (Figure 2–8).

Two endcaps (TEC) ensure a pseudorapidity coverage of $\eta = 2.5$. The endcap modules are mounted in 7 rings on 2x9 discs consisting of wedge shaped petals, each covering 1/16 of 2π. The ring detectors 1,2,5 are made of double sided modules. Each one is composed of two single sided sensors mounted back to back, one tilted by an angle of 100 mrad with respect to the other sensor giving the ϕ coordinate.

The different subdetectors (TIB, TEC, TOB, TID, BPIX, etc) are instrumented with microstrips modules in 27 different sizes and shapes. In the barrel modules are p^+ implants on a n-type bulk sensors. In the inner layers (in the barrel) and rings (in the forward) modules are $320\mu m$ thick, while in the outer layer are $500\mu m$ thick. In addition some layers and inner rings are equipped with special stereo modules for providing also z information for barrel detector and r information for disks [28].

2.3 CMS Detector Upgrade

One of the goals of the LHC is to increase the luminosity for producing more collisions and hence more interesting events, due to the fact that the most of the events produced in a collision are well studied. The increase of the luminosity also will increment the quantity of radiation considerably, in contrast the tracker performance will degrade drastically.

The operation of the LHC is subject to long periods of collider operation interleaved with shutdowns of a year or more, each in 2013 and 2016. The plan, summarized briefly, is as follows [26]:

1. **2010-2012: 7 TeV operation** to commission the LHC and the experiments and make early measurements of physics at this energy.
2. **2013/14: Long Shutdown 1 (LS1)** to repair magnet splices to allow the LHC to operate safely at 14 TeV and to improve collimation to permit operation at high luminosity.
3. **2014-2016: 14 TeV run** to explore Terascale physics at moderate luminosity within the capability of existing detectors.
4. **2017: Long Shutdown 2 (LS2)** to improve collimation in the LHC to enable operation at highest Phase 1 (period which started in March of 2010 and extends until at least 2020) luminosities; to prepare the LHC for the addition of Crab Cavities and RF cryo-systems needed for Phase 2; to connect Linac4 into the injector complex; and to upgrade the energy of the PS Booster to reduce the beam emittance.
5. **2018-2020: 14 TeV high luminosity run** to more thoroughly explore Terascale physics and to study in more detail new phenomena observed in the preceding runs using the upgraded detectors.

In the first Long shutdown 1 (LS1) it is planned to carry out a series of changes for preparing the detector to the increase of luminosity and also to hold its efficiency to the maximum. The principal changes include [26]:

- **Muon System**
  - Addition of a fourth layer of chambers and associated readout and triggering electronics to preserve a low P_T threshold for the Level 1 Muon Trigger at high luminosity.
  - Deployment of new muon trigger primitive electronics to deliver the additional muon track segments, which will be produced at high luminosity.
  - Relocation of the sector Collector board for the periphery of the detector where they are exposed to radiation and high magnetic fields, and where the cooling

is marginal to the Underground Control Room where the environment is more congenial.

  - Addition of a fourth layer of Endcap Resistive Plate Chambers (RPCs) to extend coverage to $\eta = 1.6$ to preserve a low P_T threshold for the Level 1 Muon at high luminosity.

- **Hadron calorimeters:** this upgrade will improve the efficiency and the trigger at all luminosities.
  - Implementation of depth segmentation which has advantage in coping with higher luminosities and compensating for radiation damage to the scintillators.
  - Substitution of the photomultipliers (PMTs) of the Forward Hadron Calorimeter with new photomultipliers with thinner glass windows and metal envelops to reduce the quantity of Cherenkov light generated by charged particles traversing through the glass. The Cherenkov light form the glass creates large pulse heights that look like energetic particles in the trigger and analysis.
  - The new PMTs also have 4-way segmented anodes that provide additional rejection of false signals. These PMTs also have higher quantum efficiency so the resolution of the HF will improve, and HF will last longer under irradiation.
- **Pixel System:** the present pixel detector could not maintain a high tracking efficiency at luminosities up to $2 \times 10^{34} cm^{-2} s^{-1}$ due to severe data losses in the readout chip (ROC). It was designed for operation with a maximum luminosity of $1 \times 10^{34} cm^{-2} s^{-1}$, hence the present pixel detector will be replaced with one that can maintain twice the luminosity of the current. The main features of the detector upgrade are:
  - Replacement of the current 3-layer barrel (BPIX),2-disk end cap (FPIX) system with a 4-layer, 3-disk end cap system for four hit coverage.
  - Ultra lightweight support with CO_2 cooling and displacement of the electronic boards and connections out of tracking volume for material reduction.

- Development of a new readout chip with reduced data loss at higher collision rates expected in Phase 1.
- Development of high bandwidth readout electronics and links as well as DC-DC power converters, which allow the reuse of existing fibers and cables.

The fourth barrel layer at a radius of 16 cm and the third set of forward disks will maintain the current level of tracking performance even in the high occupancy environment of the upgraded LHC. It provides a safety margin in case the first silicon strip layer of the TIB degrades faster than expected. The upgraded pixel system will have less mass than the current, this reduction in the amount of material and the increase in the number of measurement points will improve the resolution of all track parameters. In particular the resolution of longitudinal and transverse impact parameters will be significantly improved [26].

CHAPTER 3
OBJECTIVES

In the period named Phase I of the LHC, the luminosity will increase two times of the current ($\mathscr{L} = 10^{34} cm^{-2} s^{-1}$), therefore there will have an increase of the charged particle flux at various radii on the CMS tracker system. The current design of the CMS pixel detector could not keep its good performance and does not take advantage of the new luminosity, thus degrading faster than expected.

In order to maintain the optimal performance of CMS tracker, an improvement in the CMS pixel detector has been planned. The upgrade consists of an increase in the number of barrel pixel layers from three to four, and replacing the two endcap disks per side by three disks in each side. The addition of the fourth barrel layer and the third forward disks will improve the present level of tracking performance even in the high occupancy environment of the upgraded LHC. The fourth barrel pixel layer will provide an additional hit for the track reconstruction, thus improving the track seeding. Likewise a third forward pixel disk will ameliorate the coverage throughout the central tracking region.

The pixel detector plays a crucial role in the track reconstruction process, since for a track be succesfully reconstructed at least 8 hits, 3 of which are in the pixel detector (seeding) are required. The remaining amount of hits are distributed along the other two subdetectors of the tracker such as the Tracker Inner Barrel (TIB) and Tracker Outer Barrel (TOB). Therefore it is considered important to measure the impact that will have a scenario with a higher radiation on the tracker system, especially in the pixel detector due to its proximity with the collision point. For this reason, the CMS software has introduced modifications in the geometry of the tracker system such as a lighter

upgraded pixel detector and a new smaller diameter beam pipe, allowing an inner pixel layer closer to the beam spot.

To simulate the detector performance at higher luminosity conditions, we have selected two likely scenarios. The first scenario considers the temperature increase within the tracker due to high levels of radiation, particularly the regions closest to the collision point. Hence a number of modules in the outer tracker could be operating at higher temperatures than their designed temperature due to insufficient cooling. Those modules could be degraded or expected to fail in the future. This escenario is called dead modules [13]. In the second scenario the degradation of the pixel detector due to radiation damage is studied. The method proposed characterizes the irradiation effects in terms of a reduction in the electric charge collected in the readout chips of the first barrel pixel layer. Note that results shown are preliminary as the proposed model here, it is an empirical model because there is no theoretical model to simulate this effect.

The main objective of this work is to simulate the CMS tracker performance system for the current (standard) and upgrade detector (Phase I) under severe conditions as luminosity increases. The tracker performance for the two proposed scenarios is evaluated through a set of plots for tracking and trigger efficiency performance in a high pile-up scenario. In this way the design of future upgrades on the CMS tracker detectors and consequently the geometry can be optimized.

CHAPTER 4
DEGRADATION STUDIES AND CONCLUSIONS

The CMS tracker has 75 million readout channels organized in 16924 modules each one being a complete detector. A single module is identified by a unique id with the numbers giving its layer, ring and module position in the ring (phi (ϕ) coordinate). Eventually after an increase to the luminosity and an upgrade to the LHC, some of these modules will present problems and could become inactive.

We study the tracker performance with the loss of up to 675 modules in the tracker system, distributed in the tracker inner barrel (TIB), in the tracker outer barrel (TOB), and the tracker inner disk (TID). The modules of the tracker that were simulated like bad ones are summarized below (Table 4–1).

Table 4–1: Summary bad components.

BadComponent	*Modules*	*Fibers*	*Apvs*	*Strips*
TIB	495	1350	2700	345600
TID	48	144	288	36864
TOB	132	264	528	67584
TEC	0	0	0	0
Tracker	675	1758	3516	450048

In the simulation the previous modules were turned off in the tracker and simulations were run at zero and fifty pileup. The impact and subsequent degradation of the tracker will be measured through the tracking efficiency and track fake rate, both for two different geometries; standard (current detector) and phase I geometry (upgrade detector). The preliminary results on radiation damage simulation effects over the pixel detector are presented as well. As a first approximation to simulate radiation damage, the irradiation effects in terms of a reduction in the electric charge collected in the readout chips of the barrel pixel layer 1 is used. This layer was selected because of its proximity to the

interaction point, therefore it is expected to be the most affected by radiation. The results will be useful for evaluating the upgrades and the advantages of the new pixel detector.

4.1 CMS Software

CMSSW is built around a Framework, an Event Data Model (EDM), and Services needed by the simulation, calibration, alignment, and reconstruction modules that process event data so that physicists can perform analyses [29]. This framework is used by the CMS packages and is divided into subsystems. The subsystems have packages and those packages contain modules. The programming code is found in the modules [30].

During data taking the data acquisition system takes the raw data from the collisions and stores them in an EDM ROOT file, ROOT is an Object Oriented Framework containing built-in functions and user-compiled code to produce graphs, histograms, and ntuples with data objects. The EDM framework allows additional computations and analyses to be stored with the previously recorded Event, as shown in Figure 4–1.

In the reconstruction process, a computational Event is a name given to a beam crossing in the storage file. The firs step in Figure 4–1 is the digitizer, this package access and modifies the ROOT file for creating and storing a ROOT object named digis, which

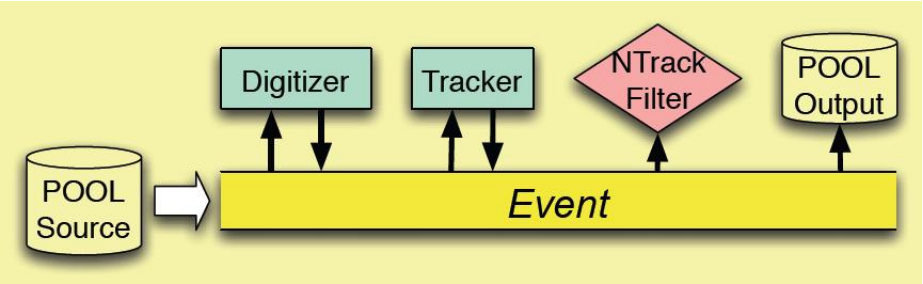

Figure 4–1: The processing model of the track reconstruction using the EDM framework in CMSSW [9].

will later be used in the hit reconstruction (Section 4.2), then the reconstructed hits are accessed by the track reconstruction modules. The track reconstruction modules will create (instantiate) a track object, finally the data is stored as an output in to the EDM root file for further analysis by the data analysis packages [30].

4.1.1 Tracker System Simulation

The tracker system is the part of the detector closest to the interaction point, hence it will be affected most by the increase in luminosity, for instance the small space available in the pixel read out chip limits the size of data buffers and the complexity of circuits, this will result in some data loss. Also pixel inefficiencies are expected due to separated or noisy pixels. These conditions are simulated in the CMS software through randomly chosen pixels, double-columns, and whole readout chips being de-activated. The data losses are dependent on the CMS trigger rate and the average number of hits per pixel (occupancy). With all these requirements the CMSSW provides users a framework that simulates the detector performance and its subdetectors, and, also possible failures (inefficiencies) [29].

4.2 Track Reconstruction

Track reconstruction is one of the most important tasks in the study of particle physics, it allows us to comprehend the fundamental aspects of the interactions that occur between the particles through the analysis of all physical quantities involved (momentum, impact parameter, mass, etc). Some important parameters used in the reconstruction of tracks are:

- Track: is the path of a charged particle as it passes throught the detector.
- Impact Parameter (d): is the closest distance between a track and the interaction point. There are two components of the impact parameter, longitudinal distance (d_z) along the beam axis and transverse distance (d_{xy}) perpendicular to the beam axis.

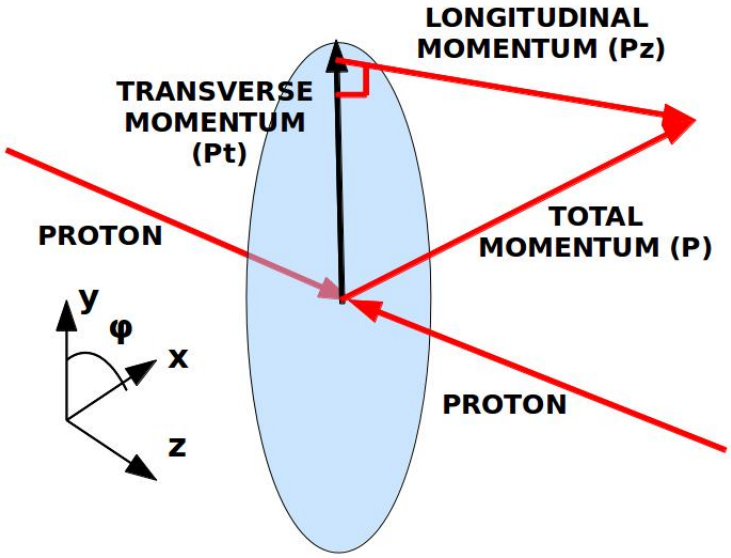

Figure 4–2: Projection of the transverse momentum of a particle on the detector transverse plane.

- Transverse momentum (P_T): the projection of the momentum of a charged particle onto the transverse plane (Figure 4–2).
- Track pseudorapidity (η): is a very useful kinematic variable. Since it is a Lorentz boost the diference between two pseudorapidty angles is invariant under any frame of reference, additionally only depends on θ, and not the mass and momentum of the particle (see section 2.1.2). In the proton-proton collision, η is related with angle between the beam line and the vector momentum of the particle (Equation 2.2).
- Hit: is a small footprint left by a charged particle in a CMS subdetector due to its interaction with the material of the sensor.

With the information provided by the CMS subdetectors, the tracker pattern reconstructs the local hit position in the silicon detectors and uses them to extrapolate the

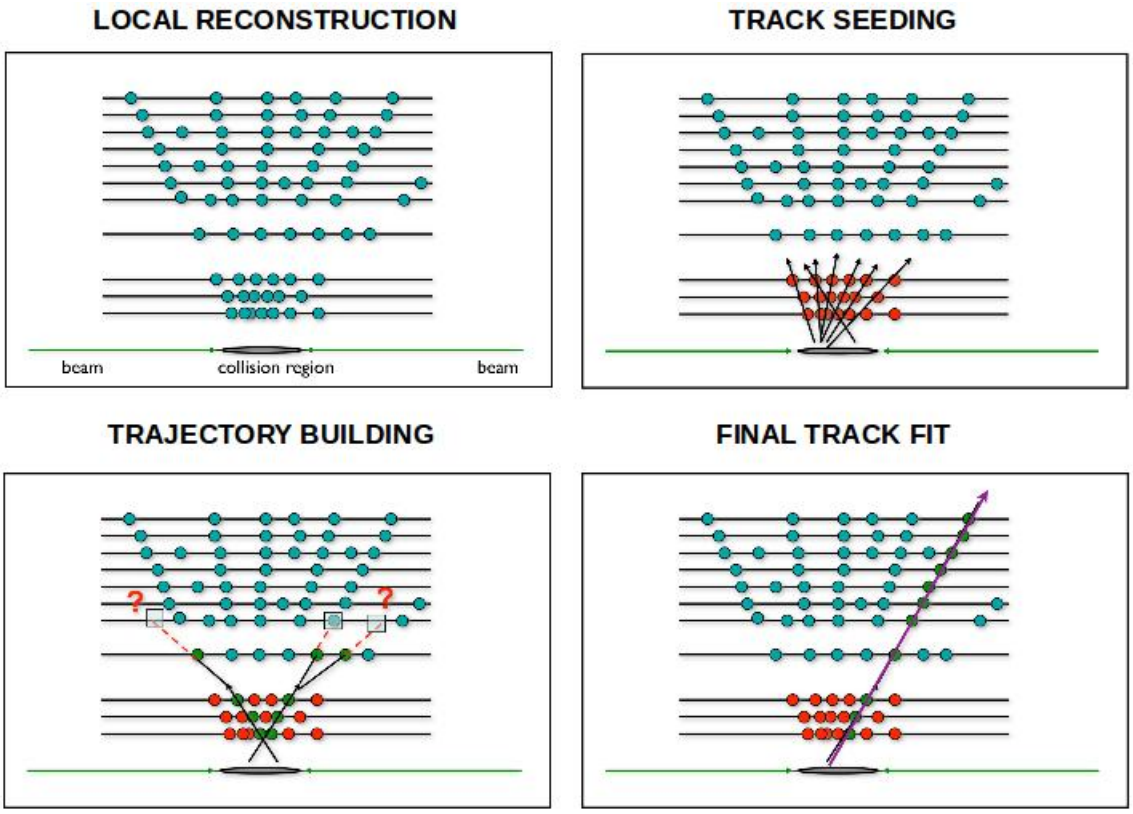

Figure 4–3: CMS reconstruction steps [10].

helical trajectories of the charged particles and provides a measurement of their momenta (P) [31]. The reconstruction process in the CMS tracker is divided into four main stages (Figure 4–3):

4.2.1 Local Reconstruction

When charged particles pass through the detector, they interact with the material which make up the sensors. The signals like charge or thermal energy are interpreted by the strips or pixels close to the interaction point of the experiment. Depending on the particle and its angle of incidence, signals with varying pulse heights are generated from the strips. In the local reconstruction process, the group of strips/pixels that are believed to originate from the same particle are clustered together. The local reconstruction

process estimates the positions of the hits and its errors from these clusters, this forms the reconstructed hits (rechit) [30].

4.2.2 Track Seeding

A subset of hits in the tracker is used as seeds to find tracks. Seeds can be pairs or triplets of hits that are compatible with the interaction region and above a P_T threshold. They are considered as possible candidates for charged tracks. These contain the information about the initial trajectories of the particles, as well as the parameters necessary for the reconstruction of tracks (transverse momentum (P_T), charge, impact parameter, etc). The estimate of these parameters should be sufficiently close to their true value to allow the use of linear fitting algorithms and uncertainties of the parameters should be sufficiently small to define a reasonably compact search region for hits. For producing seeds, two kind of methods can be used, the hit pair finding and the hit triplet finding.

- **Hit Pair Finding:** a hit pair is constituted by two hits from two different layers, with one of the hits of larger radius than the other. The search for the hit pair starts by looking for a hit on the layer that is furthest from the beam pipe (outer hit). The range of the position for the second hit is constrained analytically by using the minimum allowed momentum, possible direction of the tracks and vertex constraints. The position uncertainties caused by the multiple scattering, hit errors and the non linear projection of the helix are taken into account to widen the search window. The inner hit (second hit) should have a smaller radius compared to the first hit. The analytical constraint of its position is computed taking the vertex constraint into consideration [30].
- **Hit Triplet Finding:** this method uses the same principles as described above, however a third hit is added to the hit pair from another layer without the strict vertex constraint.

Due to limitations in the prediction of the helix track, using a hit pair is not enough to compute the transverse momentum. An additional constraint on the circular path

is needed. The track is assumed to pass through a known vertex or the center of the beamspot. The estimation uses the equation of an ideal helix passing through the hit pair and the beam axis. Once a seed is found it is extrapolated to the next layer with the uncertainties to look for compatible hits. If a compatible hit is found, the track is updated by using the additional hit, a process known as track building [30].

4.2.3 Trajectory Building

For track reconstruction it is necessary to know the basic kinematic parameters of charged particles at their point of interaction. Five parameters are considered to describe the trajectory of a particle (track) passing through the tracking system: the coordinate of the impact point in the transverse (d_{xy}) and longitudinal (d_z) plane, the azimuthal angle (ϕ) of the momentum vector of the track, the slope of the track ($\cot\theta$) and the transverse momentum (P_T) of the particle [26]. If a track is taken as a dynamic system then the five parameters that uniquely describe a track are fed in to the filtering process. The CMS Tracker has a pattern recognition algorithm based on the Kalman filter and it is called the Combinatorial Kalman filter (CKF), this is used for track fitting and iterating. The CKF is a succession of alternating prediction and filtering stages, beginning from a track seed, if more than one compatible hit is found on a layer, then two track are made, using each of the two hits. Then the tracks are propagated outward looking for compatible hits in the next layer. A track can be reconstructed with a maximum of one missing hit (when a compatible hit is not found in the intersection between the strip layer and the propagated helicoidal track). The CKF assigns a quality factor (χ^2) in each iteration, only the tracks with best quality and most number of compatible hits pass the filter step. Also the CKF includes the filtering and smoothing process. Filtering is used to estimate the state of a vectorial quantity (position, momentum) in the future using the measurements from the past. On the other hand the smoothing does the inverse process, computes the state of a vector in the past using the measurements taken up to present.

4.2.4 Final Track Fit

The final track is smoothed using a combination of the Kalman filter and fit. The fit is done using a least-squares fit in two stages. First a forward fit, inside-out from the interaction region, removes the approximations and biases of the seeding and track finding stages. A second outside-in smoother fit, yields the final best estimates of the track parameters at the origin vertex [31].

4.3 Tracking Performance in the CMS tracker

The tracker performance evaluation is an elaborated process, in which many factors are involved. I will describe each of the tools used in the development of this work.

- **The CMS software release (CMSSW)**: is the software that we used for performing our studies. The CMS track reconstruction process is based usually in six steps shown in the Table 4–2. All these steps can be seen as an iterative process for finding tracks of different quality and/or type. For example in the steps 0, 1 and 2 are the tracks built from different quality of seed pixel triplets or pixel pairs. Step 3 uses pixel triplets like steps 0 and 1 but searches for tracks displaced from the beamspot. Step 4 uses pixel and strip triplets from the first ring of the Tracker Endcap (TEC) to find tracks which have a missing hit. Also a combination of triplet strips from TIB are used in this step. Steps 4, 5 and 6 do not use pixels to create seeds and are designed to find tracks which are significantly displaced from the beamspot or tracks which do not leave sufficient pixel hits to be found in the earlier steps. In the current study some steps in the CMS iteration process have been modified. Table 4–3 has a detailed description of steps used in each of the two geometries used for this study. For current detector the iterative steps 0, 1, 2 and 4A were used. The d_{xy} cut in 4A was reduced to decrease CPU time and memory usage. For the upgrade detector the iterative steps 0, 1, 2 and 4A were used. The step 3 was used to recover efficiency in the eta region $|1.2| < \eta < |1.4|$.

Table 4–2: Parameters for each of the iterative tracking steps in the normal track reconstruction.

Iterative Steps	Seeds	P_T cut (GeV)	d_{xy} cut (cm)	d_z cut (cm)	Min. hits	Max. lost hits
0	pixel triplets	0.6	0.02	4.0	3	1
1	low p_T pixel triplets	0.2	0.02	4.0	3	1
2	pixel pairs with vtx	0.6	0.015	4.0	3	1
3	detached triplets	0.3	1.5	15.0	3	0
4A	pixel + (TEC(1 ring)) triplets	0.4	0.02	10.0	3	0
4B	BPIX + TIB triplets	0.6	1.5	10.0	3	0
5	TIB, TID, TEC pairs	0.7	2.0	10.0	6	0
6	TOB, TEC pairs	0.6	6.0	30.0	6	0

- **Sample:** in Table 4–3 the type of cuts that were applied to tracks in this study are shown. Usually there are three kind of cuts; "loose", "tight", and "high purity". Tracks that failed loose cut were dropped. Therefore tracks that pass tight or high purity cuts are recorded with a "track quality" variable (χ^2). The general idea is to let the users decide the appropriate level of cuts for their analysis. As an illustration, if your analysis has little background, but depends on a very pure sample, you would ask for high purity tracks, on the contrary if your analysis is searching for something obscure, you would ask for loose tracks [10]. The standard collections used for the studies presented here are high purity tracks. The selection criteria tuned for lower pileup conditions of 2012 data were kept as-is for these studies. This collection is used to evaluate the tracking performance in a $t\bar{t}$ montecarlo sample [13].
- **Tracking performance variables:** the performance of the tracker system is generally evaluated using two quantities, the efficiency to reconstruct a charged particle track

Table 4–3: Parameters for each of the iterative tracking steps used for the simulations of the current and Phase 1 upgrade pixel detector in this study.

Iterative Steps	Seeds	p_T cut (GeV)	d_{xy} cut (cm)	d_z cut (cm)	Min. hits	Max. lost hits
Current pixel detector						
0	pixel triplets	0.6	0.02	4.0	3	1
1	low p_T pixel triplets	0.2	0.02	4.0	3	1
2	pixel pairs with vtx	0.6	0.015	4.0	3	1
4A	pixel + (TEC(1 ring)) triplets	0.4	0.02	10.0	3	0
Phase 1 upgrade pixel detector						
0	pixel quadruplets	0.6	0.02	4.0	3	1
1	pixel triplets	0.6	0.02	4.0	3	1
2	low p_T pixel triplets	0.2	0.02	4.0	3	1
3	pixel pairs with vtx	0.6	0.015	4.0	3	0
4A	pixel + (TEC(1 ring)) triplets	0.4	0.02	10.0	3	0

(track efficiency) and the probability that a reconstructed track is a fake track (track fake rate). These are defined as follows [13]:

$$\text{Tracking Efficiency} = \frac{\text{N}^\circ \text{ of simulated tracks matched to reconstructed tracks}}{\text{N}^\circ \text{ of simulated tracks}} \quad (4.1)$$

$$\text{Track Fake Rate} = \frac{\text{N}^\circ \text{ of reconstructed tracks not matched to simulated tracks}}{\text{N}^\circ \text{ of reconstructed tracks}} \quad (4.2)$$

4.4 TIB degradation Flat Inefficiency Study

The CMS tracker package used for this study was the MultiTrack Validator (MTV). This is a validation tool used to test, validate, and debug the track reconstruction process. It produces a set of plots (efficiencies, fake rates, and resolutions) which are then used by the scientist for evaluating the tracking performance [32]. The outer pixel barrel layer in the upgrade pixel detector is much closer to the Tracker Inner Barrel (TIB) - the innermost part of the outer tracker. A homogeneous 20% loss of the tracking hit efficiency in the first two layers of TIB was selected to be simulated with up to 16% pixel ROC data loss. Also the tracking performance was done using a Monte Carlo sample of $t\bar{t}$ events with no pileup and with an average pileup of 50. The pileup 50 scenario correspond to the original nominal LHC beam conditions and to upgraded LHC conditions with 25 ns bunch spacing [13].

In Figure 4–4 the tracking efficiency is shown as a function of pseudorapidity (η) for the high purity track collection at zero (left) and fifty (right) pileup scenarios.

It can be seen that a uniform 20% inefficiency in the first two TIB layers reduces the tracking efficiency in both the current and upgrade detector. In the central region of pseudorapidity when the TIB layers are at 100% efficiency the tracking efficiency in the zero pileup scenario is approximately 94% for current detector and 96% for upgrade detector, while in the fifty pileup scenario is approximately 82% for current detector and 93% for upgrade detector. In the simulation of the degraded TIB layers the tracking efficiency at central region of pseudorapidity in the zero pileup scenario is approximately 91% for current detector and 93% for upgrade detector, while in the fifty pileup scenario it is approximately 73% for the current detector and 91% for the upgrade detector. Therefore the efficiency loss in tracking is worse at high pileup. The results show that the loss in tracking efficiency due to degradation in the TIB is less with upgrade detector than with current detector.

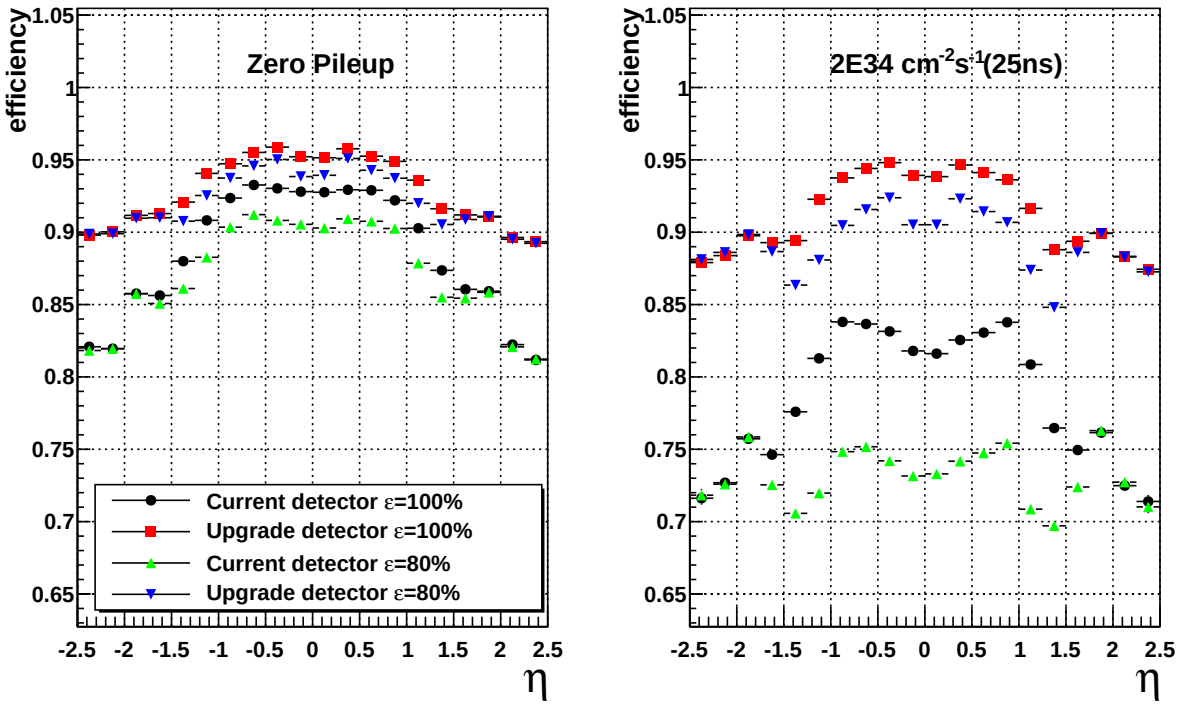

Figure 4–4: Tracking efficiency as a function of η with zero pileup (left), and an average pileup of 50 (right). Results are shown for the current detector (black circles, green triangles), and the upgrade detector (red squares, blue inverted triangles); with TIB layers 1 and 2 at 100% efficiency (black circles, red squares), and with TIB layers 1 and 2 at 80% efficiency (green triangles, blue inverted triangles).

Another way to measure the efficiency loss, is the relative loss of the tracking efficiency. This is defined as the ratio between the detector with any kind of inefficiency and the detector in optimal conditions (Equation 4.3). For instance in Figure 4–5 the ratio of tracking efficiencies with TIB layers 1 and 2 at a 80% efficiency to the tracking efficiency with TIB layers 1 and 2 at 100% efficiency is showed, this ratio would be:

$$\text{Tracking efficiency ratio} = \frac{\text{Geometry with inefficiency (TIB degradation)}}{\text{geometry at 100 \% of efficiency}} \tag{4.3}$$

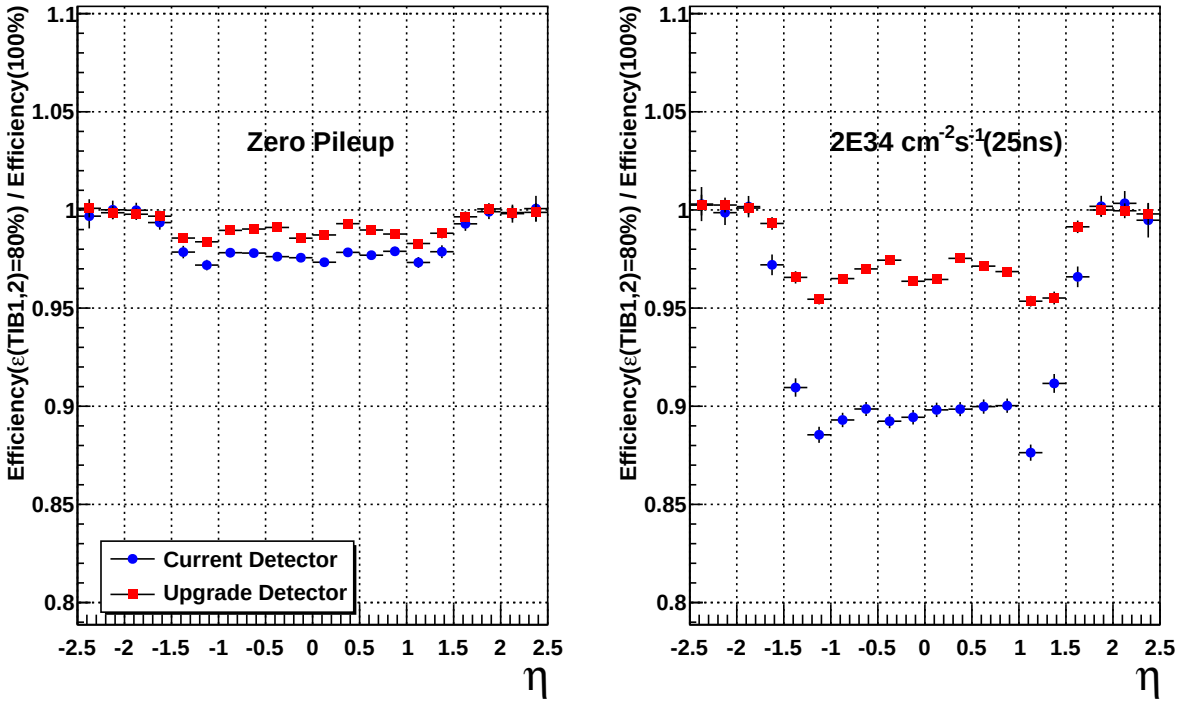

Figure 4–5: Ratio of the tracking efficiencies with TIB layers 1 and 2 at 80% efficiency to the tracking efficiency with TIB layers 1 and 2 at 100% efficiency as a function of η with zero pileup (left), and an average pileup of 50 (right). Current detector (blue circles), and the upgrade detector (red squares).

For a scenario with no pileup the relative tracking efficiency loss (Figure 4–5) is small, about 1-2% for the current and upgrade detectors. In contrast with an average pileup of 50 the relative efficiency loss with the current detector is dramatically worse at about 10%, while for the upgrade detector it is only about 4%. To account for the fact that there will be more missing hits with the degraded detector, the allowed number of missing hits was increased. Then it is foreseen that more fake tracks will be reconstructed and therefore an increase in the track fake rate is expected (Equation 4.2). Figure 4–6 shows the track fake rate for a scenario with zero pileup (left) and an average pileup of 50 (right). The track fake rates were almost negligible at zero pileup, while with an

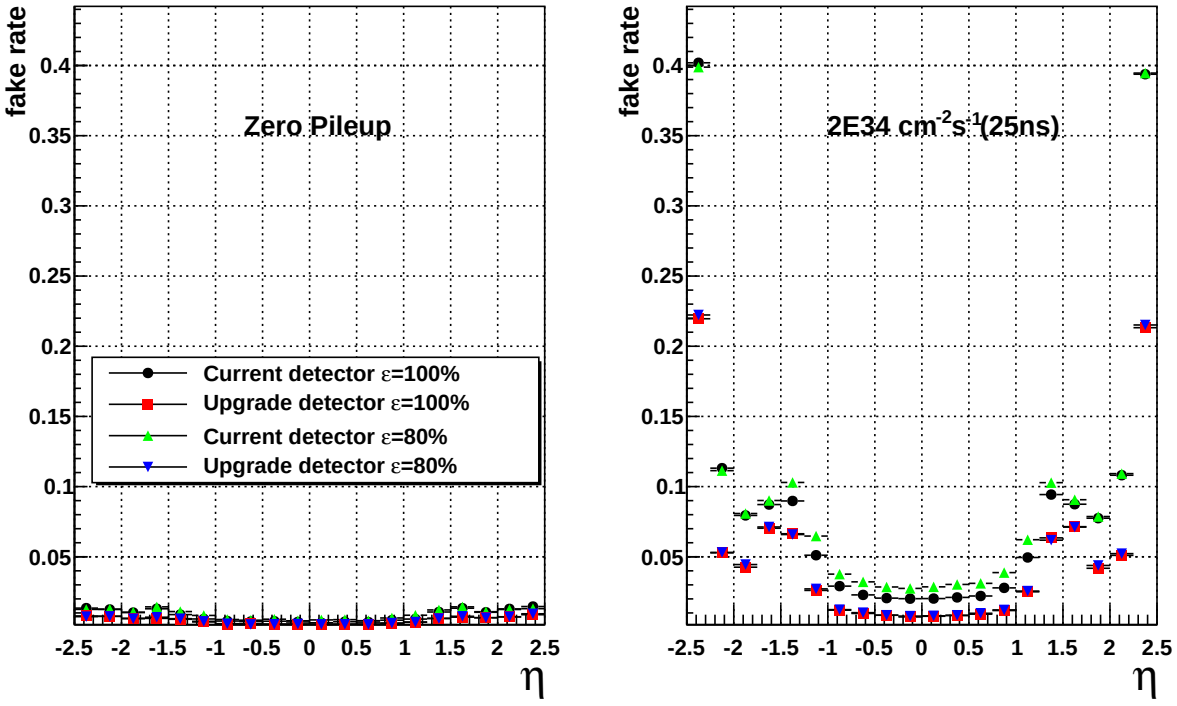

Figure 4–6: Track fake rates as a function of η with zero pileup (left), and an average pileup of 50 (right). Results are shown for the current detector (black circles, green triangles), and the upgrade detector (red squares, blue inverted triangles); with TIB layers 1 and 2 at 100% efficiency (black circles, red squares), and with TIB layers 1 and 2 at 80% efficiency (green triangles, blue inverted triangles).

average pileup of 50, the track fake rates were approximately 0.03 for current detector and 0.01 for upgrade detector with TIB layers 1 and 2 at 100% efficiency respectively. With TIB layers 1 and 2 at 80%, the track fake rates were approximately 0.04 for current detector and 0.015 for upgrade detector. Also an increase in the fake rate is oberved for the values around $\pm 1.5\eta$, this increase corresponds to the gap between the barrel and endcaps in the tracker barrel. The simulation studies shows that the track fake rate increases when the TIB degrades in performance. Figure 4–7 show the gain in fake rate with the degradation in the TIB. For a scenario with no pile up, the statistic errors do not allow reliable inferences about the degradation in the TIB (since the values for

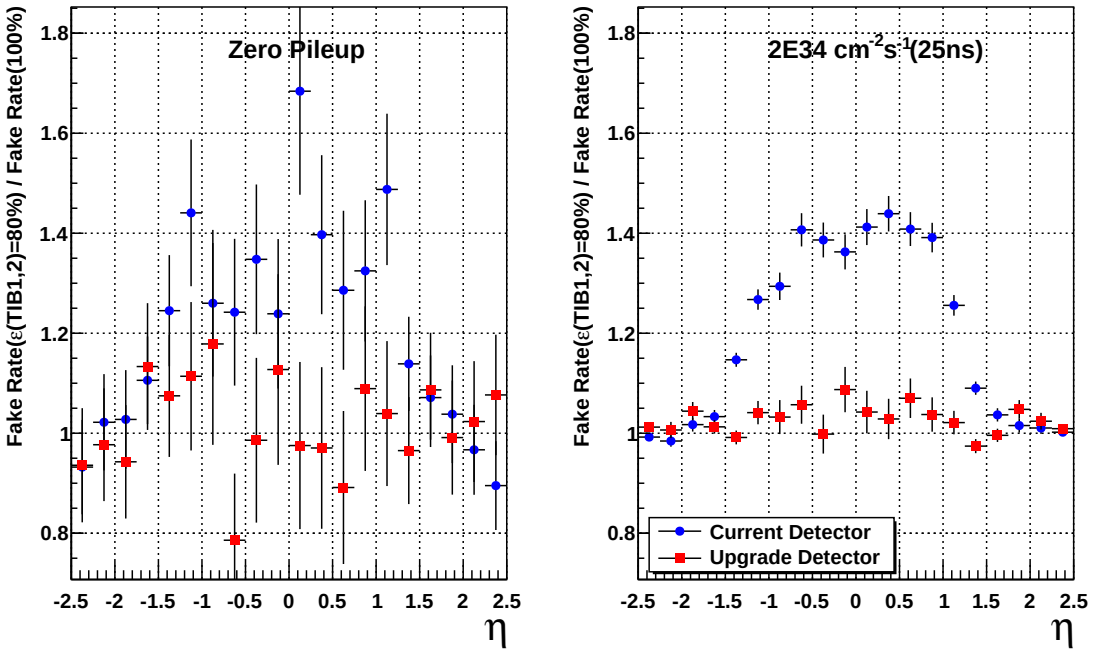

Figure 4–7: Ratio of the track fake rates with TIB layers 1 and 2 at 80% efficiency to the track fake rates with TIB layers 1 and 2 at 100% efficiency as a function of η with zero pileup (left), and an average pileup of 50 (right). Current detector (blue circles), and the upgrade detector (red squares).

the ratio between fake rates tend to zero (Figure 4–6), however at an average pileup of 50 the inefficiency in the TIB causes an increase in the track fake rate for the current detector by as much as 40%, while with the upgrade detector the increase is around 8%. These results shown that the upgrade pixel detector can mitigate the increase in track fake rates for a degradation in the TIB efficiency.

4.5 Tracker degradation produced by dead modules failure

The CMS tracker can be visualized with a specialized 2D representation of the tracker called "Tracker Map"where all modules are represented in a single screen. The trackermap is a conglomeration of 43 small images each one representing a layer/disk. The disks/layers have a set of rings. Rings are sets of modules arranged as rings in the

case of endcap disks and squares in the case of barrel cylinders. Some rings are made by modules glued back to back (stereo modules). A single module is identified by a unique id with the numbers giving its layer, ring and module position in the ring or layer. The layout of the CMS Tracker Map is shown in the Figure 4–8, each layer/disk position is represented by four parameters z and ϕ for the barrels and x and y for the endcaps [33]. In this study, the performance of the upgrade pixel detector was tested in a

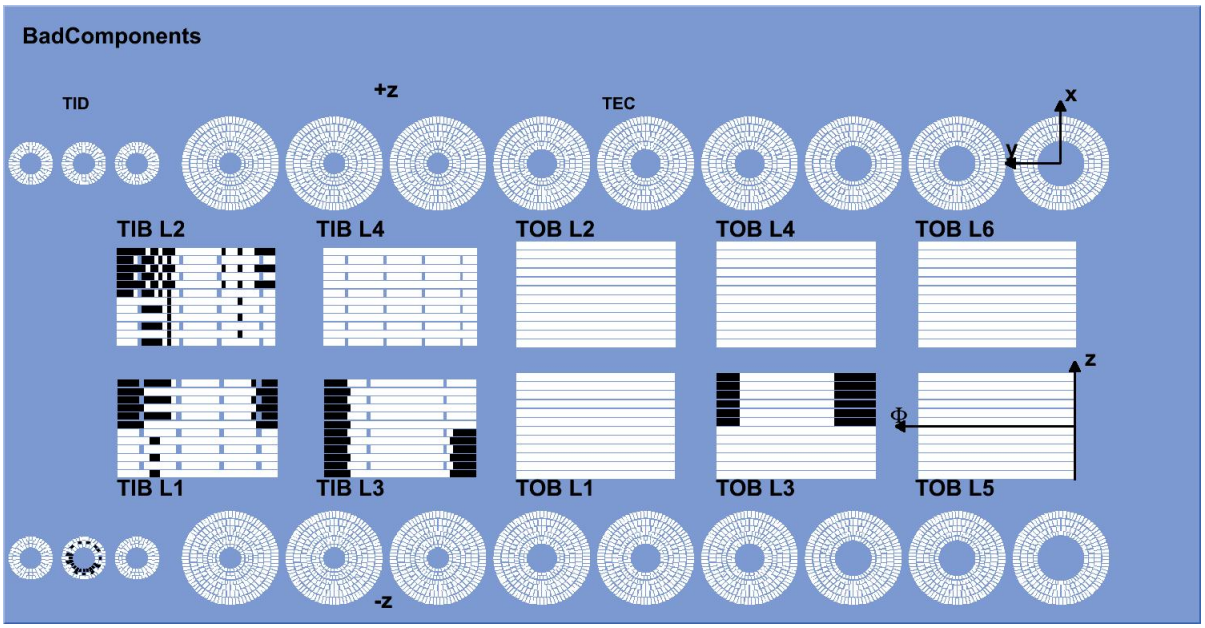

Figure 4–8: Layout of CMS Tracker Map showing modules in black that are expected to degrade in performance in the future.

more realistic scenario, where the outer tracker was also degraded. A number of modules in the outer tracker are currently operating at higher than design temperatures due to insufficient cooling, and are either degraded or expected to degrade in the future [13]. In the simulation the modules indicated in Figure 4–8 were switched off instead of using a 20% inefficiency in the first two TIB layers. Hence CMSSW will not reconstruct hits for these modules. The analysis of the impact of degradation on the tracker system is done with the parameters of tracking efficiency and fake rate, mentioned previously. A

clearer layout of the number of modules and their respective location are illustrated in the enclosed regions of the CMS tracker shown in Figure 4–9.

In Figure 4–10 the tracking efficiency is shown as a function of pseudorapidity η for the

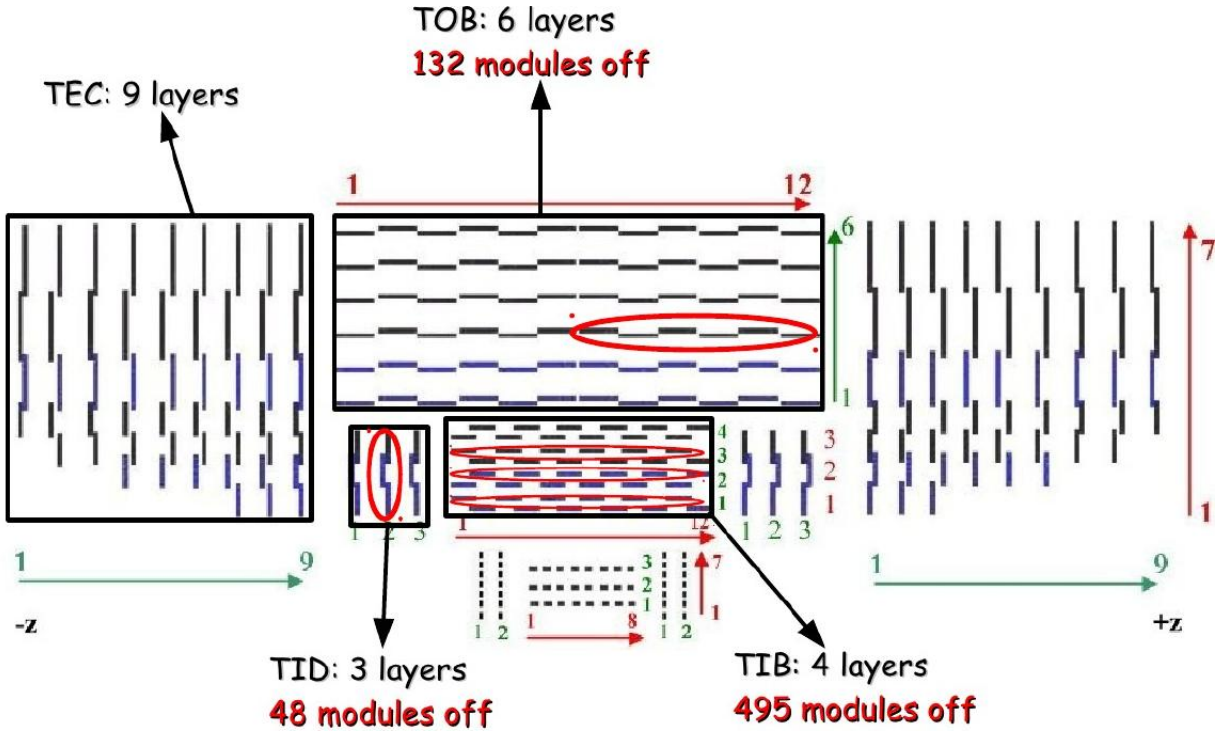

Figure 4–9: Transverse layout of CMS tracker with the number of modules switched off and their location inside of the tracker system (red ellipses). The endcap layers are numbered from 1 to 9 along -z axis, while the barrel layers from 1 to 3 for pixel detector, from 1 to 4 for TIB and from 1 to 6 for TOB along +y axis. The endcap rings are numbered from 1 to 7 starting from the centre of the petals support, while the barrel rings from 1 to 12 for TIB and TOB, from 1 to 8 for pixel detector, all along axis -z [11].

high purity track collection at zero pileup (left) and an average pileup of 50 (right).

It can be seen that switching the modules off in the zones showed in Figure 4–8 reduces the tracking efficiency dramatically in the $+\eta$ region in both the current and the upgrade detector. In the central region of pseudorapidity when the tracker modules are at 100% efficiency the tracking efficiency at zero pileup scenario is approximately 94% for current detector and 96% for upgrade detector, while with an average pileup

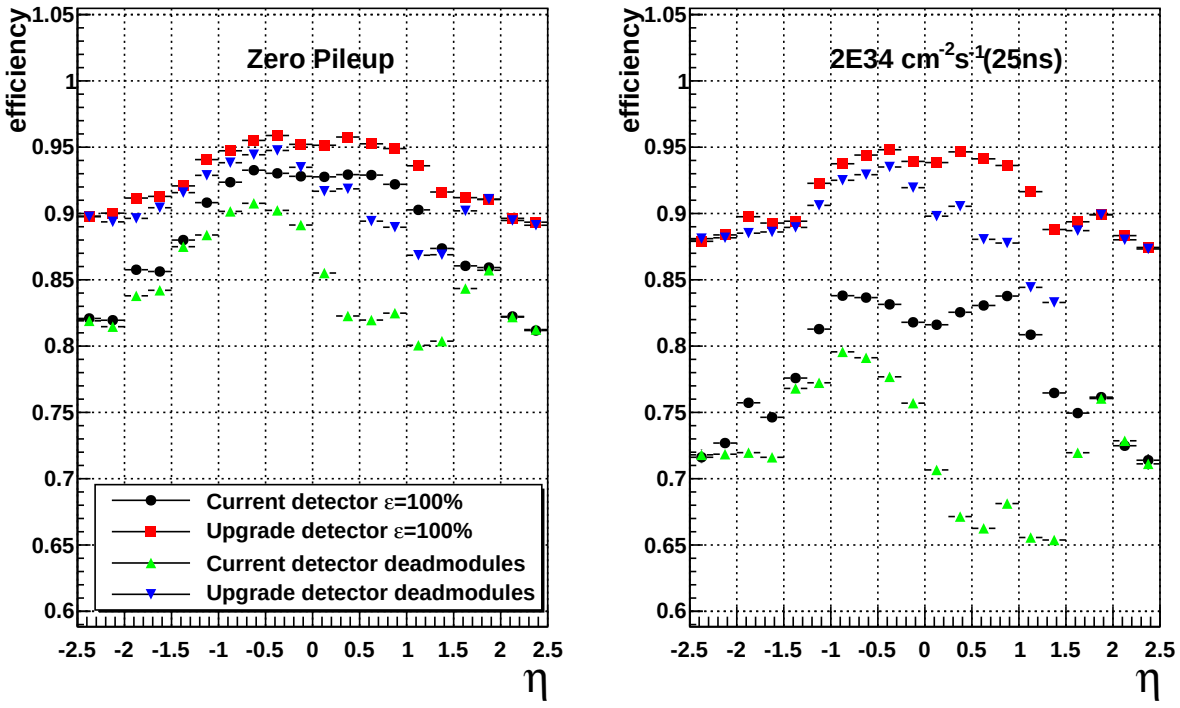

Figure 4–10: Tracking efficiency as a function of η with zero pileup (left), and an average pileup of 50 (right). Results are shown for the current detector (black circles, green triangles), and the upgrade detector (red squares, blue inverted triangles); with Tracker modules at 100% efficiency (black circles, red squares), and with dead Tracker modules (green triangles, blue inverted triangles).

of 50 scenario is approximately 82% for current detector and 94% for upgrade detector. In the case with dead Tracker modules, the tracking efficiency in the positive region of pseudorapidity in the zero pileup scenario drops dramatically to 80% for current detector and 86% for upgrade detector, while with an average pileup of 50 it is approximately 65% for the current detector and 83% for the upgrade detector. Therefore the efficiency loss in tracking is worse in the positive η region due to the amount of modules switched off in this region. However, the results shows that the tracking efficiency loss due to the tracker dead modules is mitigated for the upgrade detector in both scenarios.

Figure 4–11 shows the ratio of tracking efficiencies with dead tracker modules to the

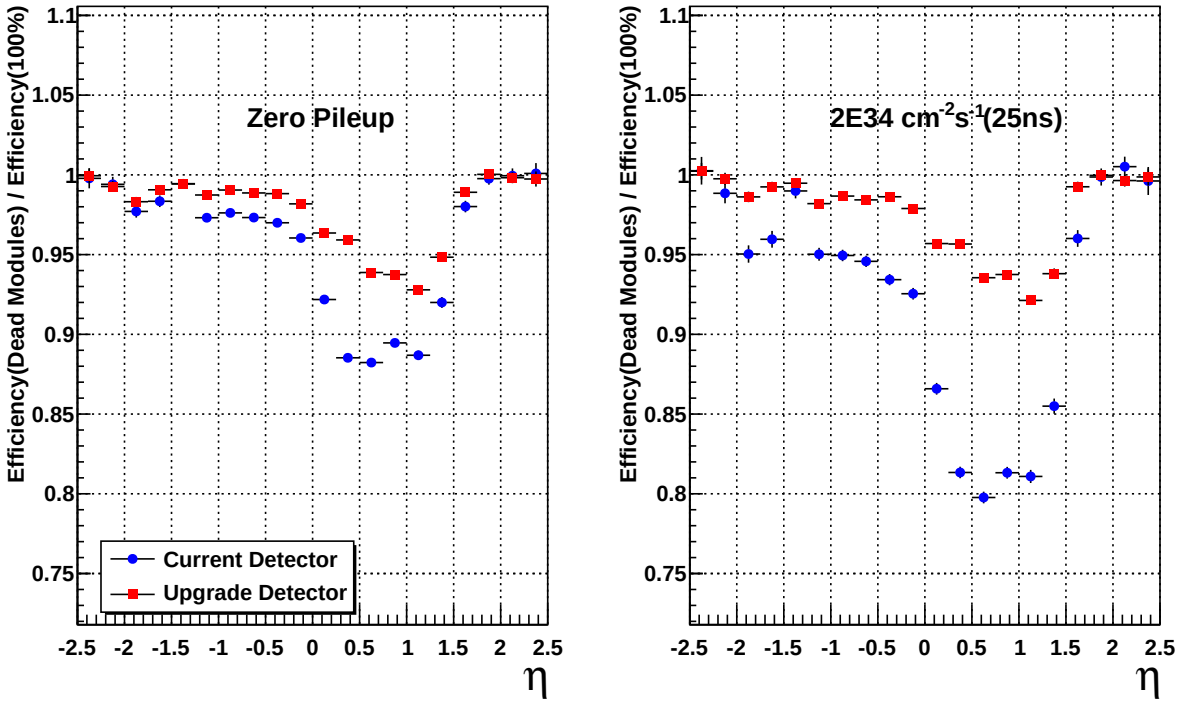

Figure 4–11: Ratio of the tracking efficiencies with dead Tracker modules to the tracking efficiency with Tracker modules at 100% efficiency as a function of η with zero pileup (left), and an average pileup of 50 (right). Current detector (blue circles), and the upgrade detector (red squares).

tracker modules at 100% efficiency. For zero pileup, the relative tracking efficiency loss is small for the negative pseudorapidity region for both detectors. On the other hand in the positive pseudorapidity region it is approximately 12% for current detector and 7% for the upgrade detector. Additionally for an average pileup of 50, the relative efficiency loss for the current detector is approximately 20% while for the upgrade detector it is only 8% in the positive region of pseudorapidity. The simulation results show that the relative tracking efficiency loss due to dead tracker modules is reduced in the upgrade detector compared to the current detector.

Figure 4–12 shows the track fake rates for the scenarios with zero pileup (left) and an

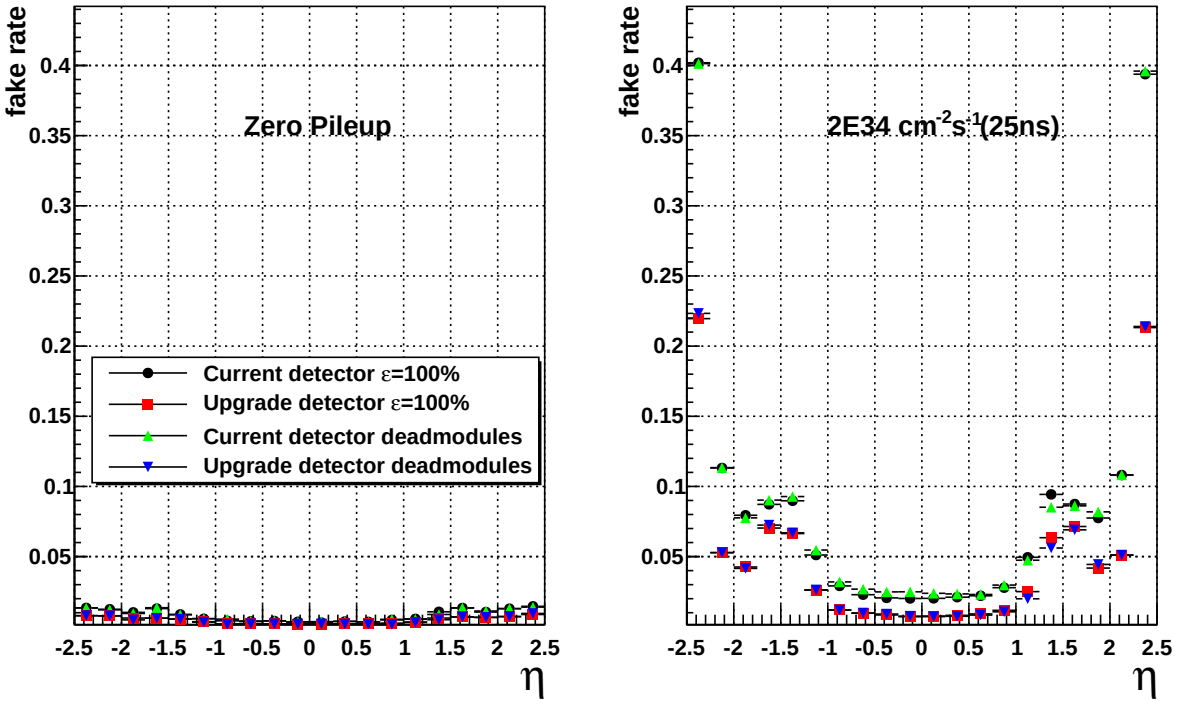

Figure 4–12: Track fake rates as a function of η with zero pileup (left), and an average pileup of 50 (right). Results are shown for the current detector (black circles, green trangles), and the upgrade detector (red squares, blue inverted triangles); with Tracker modules at 100% efficiency (black circles, red squares), and with dead Tracker modules (green triangles, blue inverted triangles).

average pileup of 50 (right). For both detectors the track fake rates are almost negligible at zero pileup. At an average pileup of 50 and the tracker modules at 100% efficiency, the track fake rates were 0.020 for current detector and 0.008 for the upgrade detector, while with the dead tracker modules, the track fake rates were approximately 0.022 for current detector and 0.010 for the upgrade detector.

Figure 4–13 shows the relative gain in fake rate with the degradation in the TIB. The track fake rates are almost negligible at zero pileup (again the values for the ratio between fake rates tend to zero (Figure 4–12) and the statistic error is increased), while with an average pileup of 50 the dead tracker modules causes an increase in the track

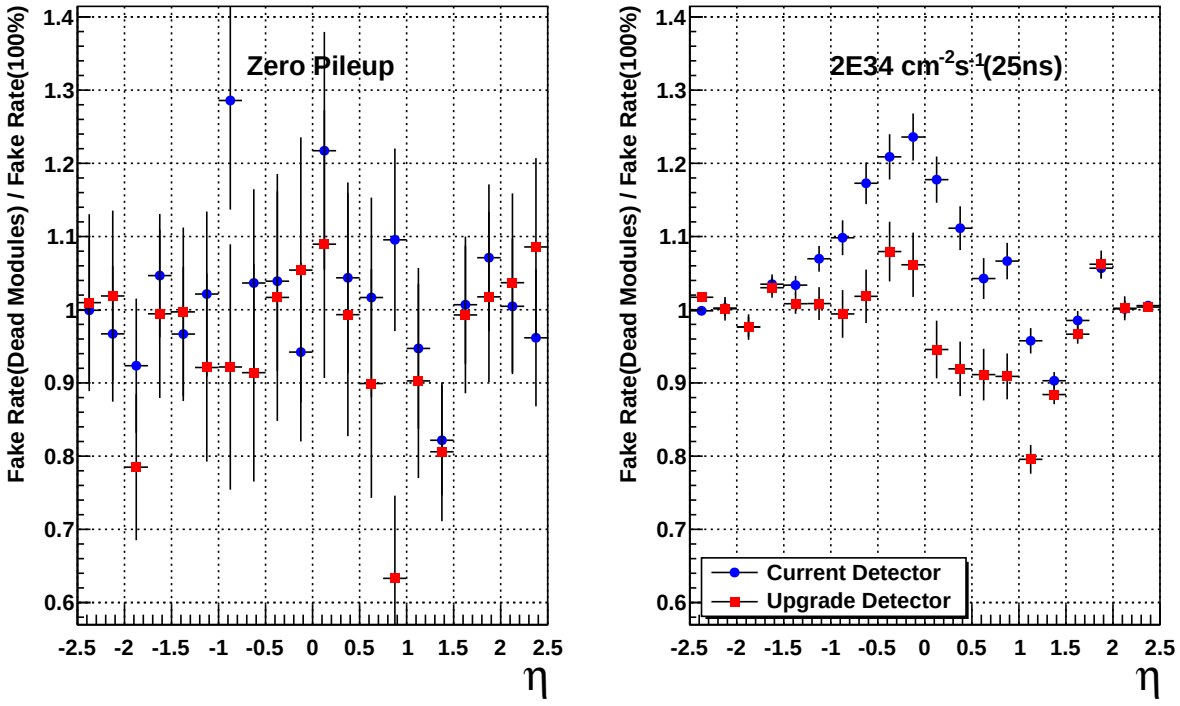

Figure 4–13: Ratio of the track fake rates with tracker modules at 100% efficiency to the track fake rates with dead tracker modules as a function of η with zero pileup (left), and an average pileup of 50 (right). Current detector (blue circles), and the upgrade detector (red squares).

fake rate for the current detector by as much 24% and 8% for the upgrade detector. These results show the ability of the pixel upgrade detector to ameliorate inefficiencies in the CMS Tracker Inner Barrel (TIB) detector.

4.6 Simulation of charge loss of irradiated pixel sensors

The performance of pixel detector under high luminosity conditions was demonstrated in the previous studies. To simulate this effect, the TIB layers closest to the pixel detector were degraded and some modules belonging to the outer tracker were turned off. In this study I proposed a method to simulate the degradation on the pixel detector due to radiation damage. This work is still in progress, and in the near future will be included in the standard distribution of the CMS software as a tool to make comparisons between the different tracking geometries (current and upgrade detector).

4.6.1 Radiation damage method

The pixel detector response is simulated by determining the length of a track along the active area of the detector (sensor) which is then divided into several segments. Each segement contains a free electric charge q which is proportional the energy loss per unit path-length (dE/dx) of the track. This charge drifts, by the influence of the electric and magnetic fields, to the detector surface where it is collected and the signal is sent to the readout chips [34]. The method proposed here simulates the irradiation effects in terms of a reduction in the electric charge collected in the readout chips of the first barrel pixel layer. This layer is considered because it will receive the most irradiation. The method uses exponential functions to describe the attenuation of charge as a function of the depth along the track length. The exponential functions are defined according to the orientation of pixel modules in the inner and outer pixel barrel layers (Equations 4.4 and 4.5).

Figure 4–14 shows how the charge is deposited in the pixel barrel detectors at the inner and outer radius once a track has passed through the active regions of the pixel detector. It is expected that in the inner radius, where the sensor is flipped, the attenuation is reduced at greater depth. Accordingly the mathematical function used for simulating

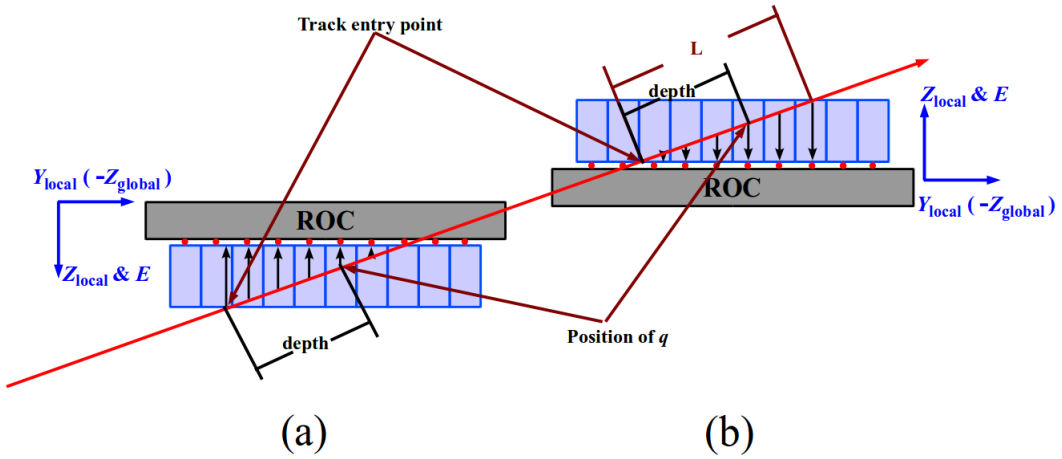

Figure 4–14: Deposition of charge by a track in the pixel barrel detector at (a) a flipped module (Inner radius) and (b) an unflipped module (Outer radius). Also are shown the pixel local coordinates.

the charge collection in a flipped pixel sensor is:

$$q = q_0 \; e^{-k(L-depth)/L} \tag{4.4}$$

where q_0 is the initial charge, q is the charge collected after radiation damage, the attenuation factor k is assigned according to the expected number of particles per unit area traversing the pixel layer [35] (integer greater than zero), L is the length of the track inside the sensor, and the "*depth*" defined as the distance from the entry point to point where the charge is located. On the other hand for the outer radius (unflipped sensor), it is expected that at greater depth the attenuation is higher, accordingly the exponential function used is:

$$q = q_0 \; e^{-k(depth)/L} \tag{4.5}$$

4.6.2 Charge Collection

In Figures 4–15 and 4–16 the charge profile for the non-irradiated and the irradiated case obtained using different methods are shown. Figure 4–15 shows the average charge collected for the layer 1 of the pixel barrel. This plot was obtained through the simulation developed in this work.

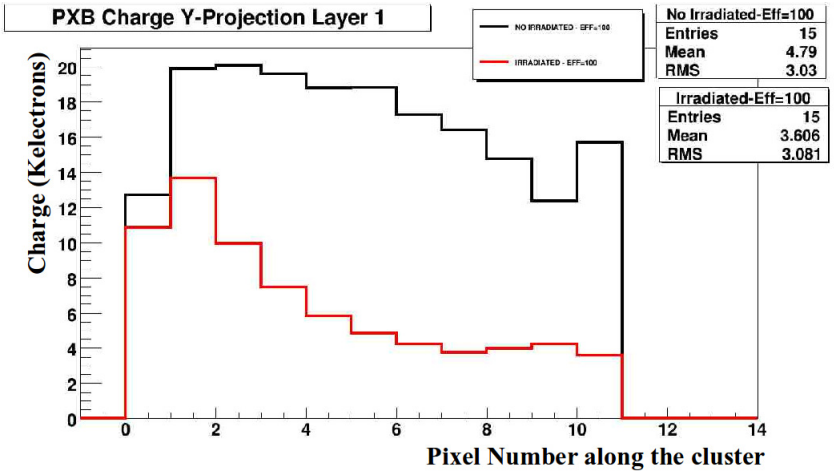

Figure 4–15: Y-projection average charge for all the reconstructed clusters with 14.9< β <15.3.

Figure 4–16 is the result of a test beam using a grazing angle of 15°. In this distribution each bin of the horizontal axis is the full average pixel signal for 8 different bins of track entry point [12]. The charge distributions show that there is a deficit in the charge collected by the sensor due to the effects of the radiation damage on the pixel modules. However, there is a fundamental difference in how we simulate the charge collection and the current algorithm used by CMSSW. The CMS algorithm computes the reduction in the collected charge by dividing the track of the particle in several segments, then to minimize charge fluctuations, only the charge deposited in the entry and exit point is considered, the charge distribution in the inner pixels is supposed to be flat. Our algorithm computes the collected charge by taking the charge deposited in the initial and exit point, then a decrease or exponential increase in the charge collection is assumed. Currently we are working in adding some physical parameters in the code that allow us a best fit in all these distributions to reproduce the reduction in the size of the cluster due to radiation damage.

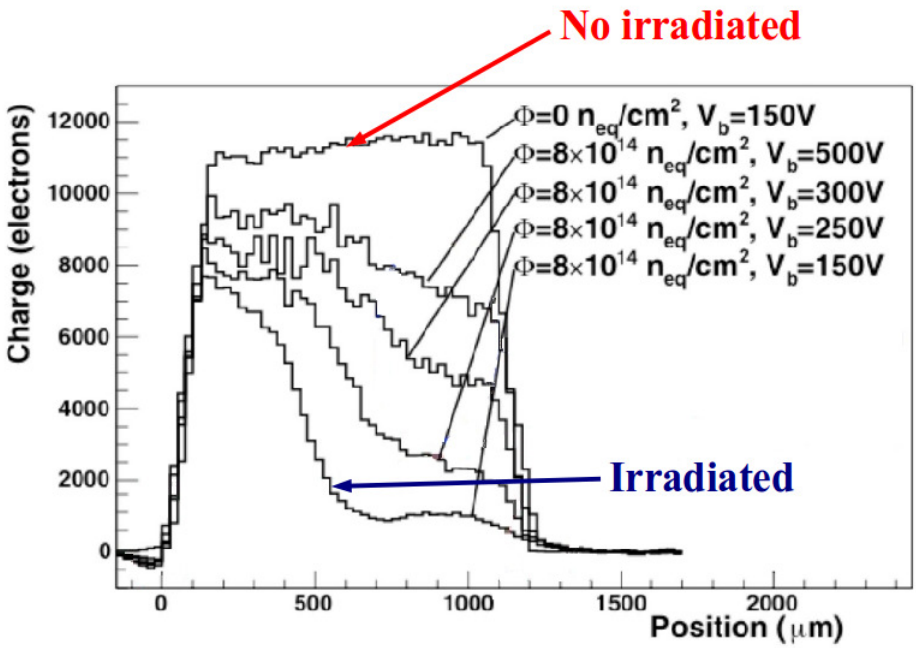

Figure 4–16: Charge Y-Projection for sensors of $125\times125\mu m^2$ illuminated by a $\beta = 15°$ test beam [12].

4.6.3 Pixel Hit Resolution Study

The point where the charged track interacted with the pixel sensor is known as hit position. Estimates of the hit position in the pixel sensor requires knowledge of the cell size, the charge measured by a single pixel, the charge shared between pixels and the readout threshold in the pixel sensor. The precision with which hit position is estimated is called pixel hit resolution or spatial resolution. The pixel detector in CMS, is the only one able to measure the hit position in two dimensions. With the help of the Lorentz angle ("the angle by which particles moving in an electric field are deflected due to the effect of a magnetic field" [36]), the particle trajectory is extrapolated and therefore reconstructed. By increasing the particle flow (fluence) in the detector, the Lorentz angle will become smaller due to high radiation decreasing the charge sharing and consequently the spatial resolution.

Figures 4–17 and 4–18 show the pixel hit position resolution for the current detector

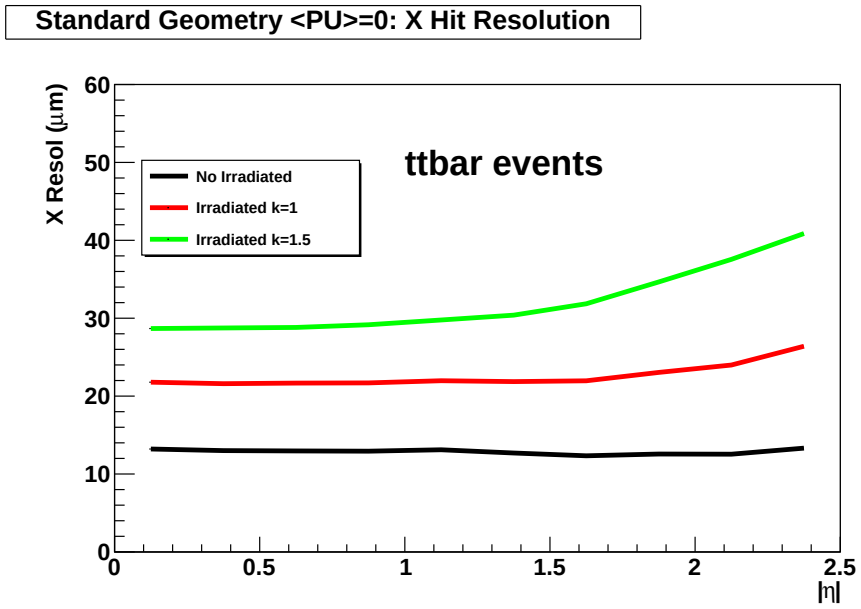

Figure 4–17: Pixel X hit position resolution as a function of the pseudorapidity $|\eta|$. No irradiate case (black solid line), for an attenuation factor of $k = 1.0$ (red solid line) and for an attenuation factor of $k = 1.5$ (green solid line).

as a function of pseudorapidity $|\eta|$ for the non-irradiated and irradiated cases, these illustrate how the radiation damage affect the spatial resolution in the layer 1 of the pixel barrel. Each one of the attenuation factors used in the simulation correspond to the values in the integrated luminosity computed for the layer 1 of the pixel barrel. In this case $k = 1.0$ corresponds to an integrated luminosity value of $\mathscr{L} \sim 250 fb^{-1}$ and $k = 1.5$ corresponds to an integrated luminosity value of $\mathscr{L} \sim 500 fb^{-1}$. The results in the longitudinal pixel hit resolution (Figure 4–17) and transverse pixel hit resolution (Figure 4–18) are the expected, for low values of the pseudorapidity a good resolution is maintained because in this region the clusters are wider in eta (Figure 4–19). For high values of the pseudorapidity after irradiation ($k = 1.0$ and $k = 1.5$), the radiation damage plays an important role in the "breakage" of clusters. In this region the tracks traverse the pixel cells along the beam axis (Y hit position) direction producing long clusters. These clusters can "break" into separate clusters as more charge is lost [13],

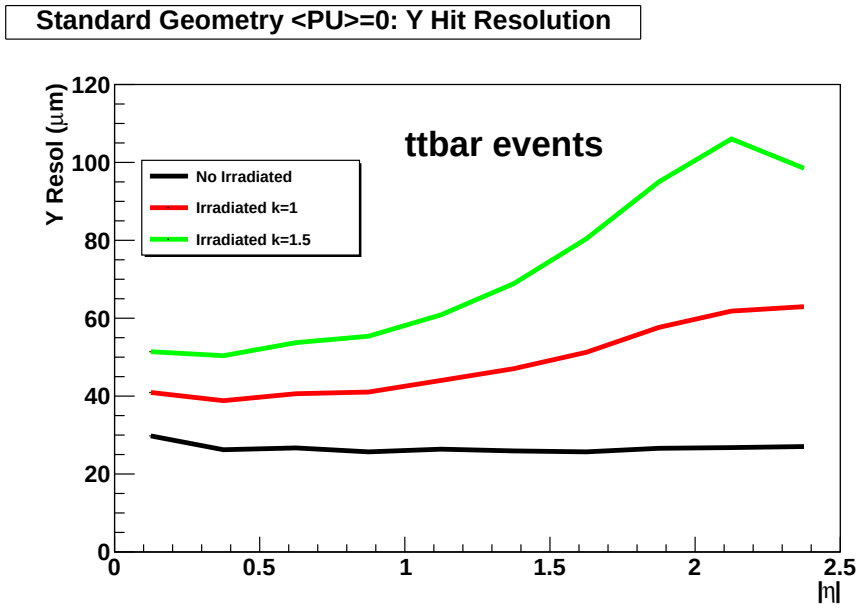

Figure 4–18: Pixel Y hit position resolution as a function of the pseudorapidity $|\eta|$. No irradiate case (black solid line), for an attenuation factor of $k = 1.0$ (red solid line) and for an attenuation factor of $k = 1.5$ (green solid line).

consequently the resolution is degraded. However more studies are needed to determine whether results match to those obtained by PIXELAV simulation [37]. This is a more detailed simulation of the phenomenon studied here but is not integrated into CMSSW.

4.6.4 Primary Vertex Resolution Study

The vertex reconstruction process is an important task for studying jets and btagging physics in experiments at high energy colliders like CMS. Good Vertex reconstructing allows for the effective separation of secondary vertices from the primary vertices. The Phase 1 of the CMS pixel upgrade is expected to operate in an environment with an average of $20-40$ pp interactions per bunch crossing. Hence an efficient and accurate vertexing is required, in addition associating individual tracks to vertices with precision allows the separation of the most interesting events from the well studied events. Figure 4–20 shows the transverse and longitudinal primary vertex resolution as functions

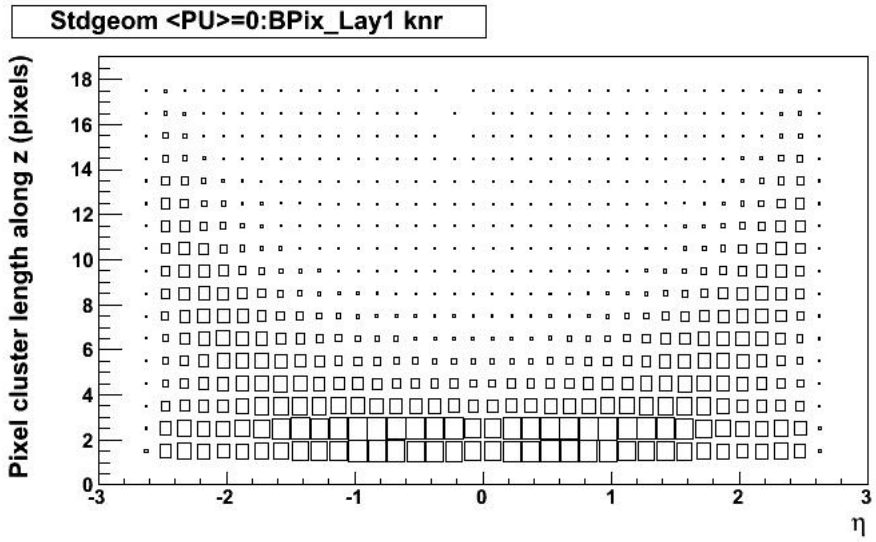

Figure 4–19: Size of the cluster (set of pixels) in the layer 1 of pixel detector along the z coordinate as a function of η for a non-irradiated sensor (knr). It can be appreciated that at high η values the clusters are larger, up to 16 pixels

of the number tracks for the current detector at zero pileup. These were the results of simulating radiation damage on the layer 1 of the pixel barrel. The lower part of each plot shows the ratio of $k = 1$ resolution to the non-irradiated resolution (black squares) and the ratio of $k = 1.5$ resolution to the non-irradiated resolution (blue squares) for the transverse and longitudinal primary vertex resolution respectively (Figure 4–20 (a) and (b)). The ratios of the resolutions show a resolution loss for the current detector produced by radiation damage, in addition when the attenuation factor is increased the resolution loss becomes more dramatic. Figure 4–21 shows the transverse and longitudinal primary vertex resolutions as a function of the number of tracks in the vertex for a $t\bar{t}$ sample for a non-irradiated sensor. These plots were obtained with the CMSSW standard code, ie, the radiation damage is not included. The results for a non-irradiated sensor at zero pileup are compared. Figure 4–20 (a) shows that the transverse resolution loss in the primary vertices for a low number of tracks is about 20 μm (red squares) respect to the same study in Figure 4–21 (black circles (left-top)). This means that for low track numbers, the simulation proposed here is still far from the standard CMSSW

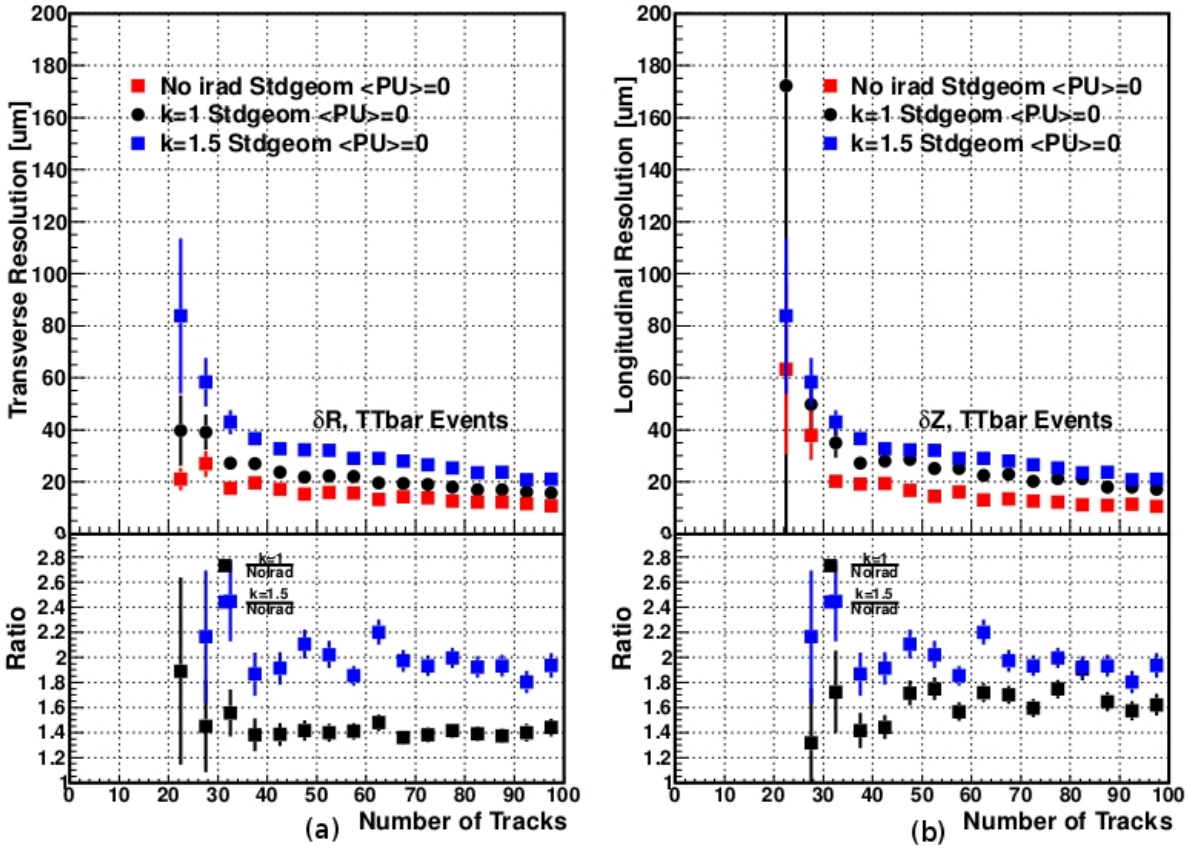

Figure 4–20: Transverse (a) and longitudinal (b) primary vertex resolutions (top) as functions of number of tracks in the vertex for a $t\bar{t}$ sample with zero pileup. The resolutions are shown for the current pixel detector no irradiated (red squares), radiation damage with exponential functions for $k = 1$ (black circles) and $k = 1.5$ (blue squares).

simulation, nevertheless with increasing the number of tracks, the simulation of radiation damage by exponential method behaves similar to the standard. Similarly the longitudinal resolution loss in the primary vertices for zero pileup (Figure 4–20 (b) (red squares))with the method proposed here, is around 35 μm respect to the same study in Figure 4–21(black circles (bottom-left)) for zero pileup. However as increases the number of tracks, the simulation behaves in the same way as the CMSSW standard. Currently we are working on improving some aspects of the simulation to obtain results closer to those observed in other studies [12].

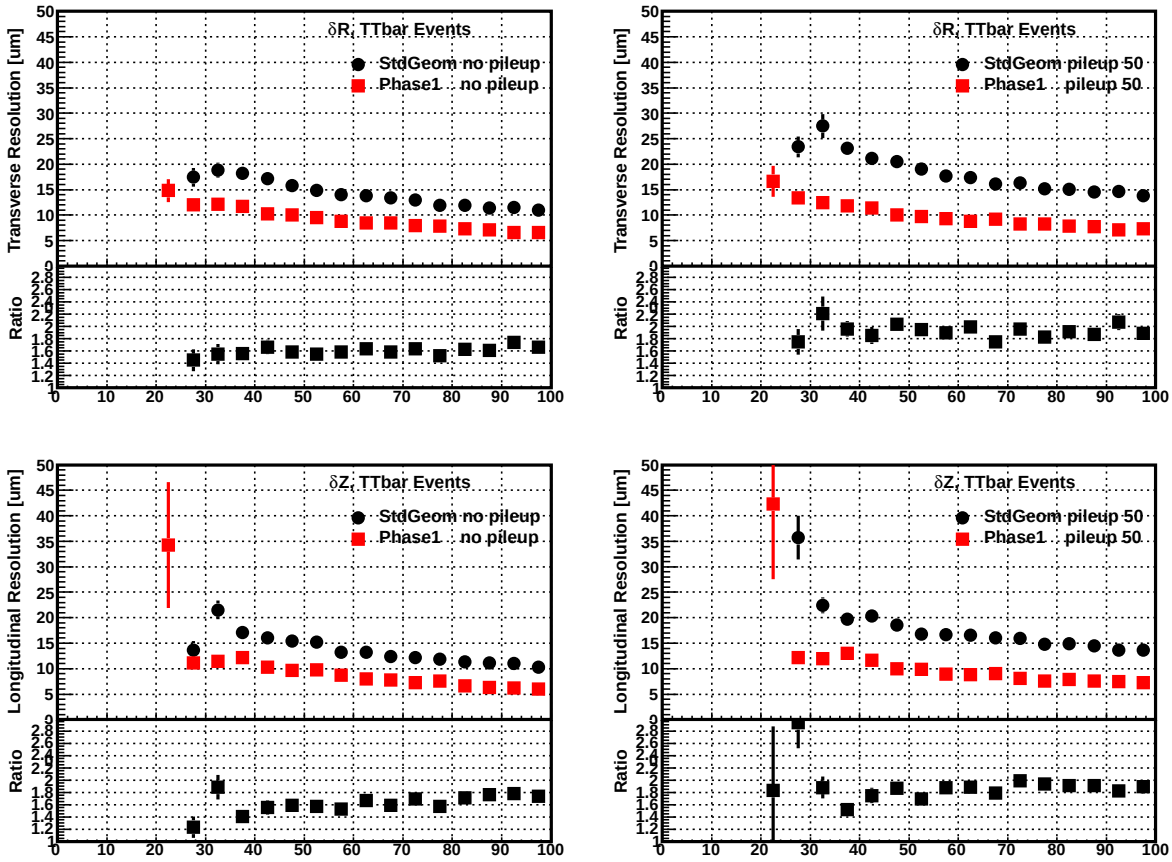

Figure 4–21: Transverse (top) and longitudinal (bottom) primary vertex resolutions as a function of the the number of tracks in the vertex for a tt sample with (left) zero pileup, and (right) with an average pileup of 50. The resolutions are shown for the current pixel detector (black circles) and the Phase 1 upgrade detector (red squares). The lower part of each plot shows the ratio of the current detector resolution to the upgrade resolution [13].

CHAPTER 5
CONCLUSIONS

This work presented degradation studies of CMS tracker system for the current pixel detector and upgrade pixel detector for the zero pileup and an average pileup of 50. These included a homogeneous 20% uniform inefficiency in the two first layers of the TIB, inefficiency due to failure of some modules selected inside of the outer tracker system and the radiation damage simulation in the first layer of the pixel detector. These studies analized the robustness of the upgrade pixel detector and current pixel detector to the outer tracker inefficiencies and radiation damage in the pixel detector. To evaluate the tracking performance, we compared the track finding efficiency and the fake rate in two running scenarios. The first one was at low luminosity conditions (zero pileup or no pileup) and the second one was for high luminosity conditions (fifty pileup). For the outer tracker studies, the relative efficiency loss was always worse at higher luminosity (fifty pileup with ROC data loss) for the current detector 13%(20%) than for the upgrade detector 6%(8%) for flat inefficiency (dead modules). The track finding efficiency loss was about half for the upgrade detector compared with the current detector. Likewise it was expected that the track fake rate was always worse for the current detector 40%(25%) than for the upgrade detector 5%(8%) at higher luminosity for flat inefficiency (dead modules). The track fake rate with the upgrade detector is hardly affected by outer tracker inefficiencies while it will increase substantially for the current detector.In addition the extra pixel layer in the upgrade detector showed that it can reduce the efficiency loss by more than half with respect to the current detector for a $t\bar{t}$ sample. Also the fourth pixel layer decreased the track fake rate with the upgrade detector by more than 40% compared to the current detector in the η central region. Hence the results show that the upgrade pixel detector is much more robust to outer

tracker inefficiencies than the current detector. The preliminary results of the radiation damage simulation shows that we have a good approximation for simulating the results obtained by PIXELAV (around 20%). The simulation presented here ran much faster than the PIXELAV simulation, which is an advantage in CPU time.

5.1 International Conferences

The results of this work were presented and socialized in two international events. In the *APS High Energy Physics meeting* on April 2012 in Atlanta (USA) and the *International School On High Energy Physics* (LISHEP) on March 2013 at Rio de Janeiro (Brazil). The feedback of these meetings was very important to improve the quality of the present work.

5.2 Future Work

It is suggested that the code for the tracker dead modules be included in the standard release of CMSSW to make deeper studies in which other outer tracker modules can be switched off and therefore to possess a wider range of dead regions in the strip detector to be analized. Likewise it is highly recomendable to continue with the radiation damage study, since this is a very good alternative for simulating this effect with less CPU resources than PIXELAV. In addition once the method is validated, it can be used for studies to find tracking efficiency, fake rate, btagging efficiencies [12] and impact parameter resolutions both the current detector as the upgrade detector at zero and fifty pileup. Finally it is important to continue this study because this is a method totally new and has great potential to be used in more studies.

REFERENCES

[1] T. Han. *Collider Physics: From basic knowledge to new physics searches*. Presentation the 9th Workshop on Particle Physics Phenomenology National Central University, june 2011. http://www-het.phys.sci.osaka-u.ac.jp/lecture/hagiwara/1106ppp9than-cut-kh.pdf.

[2] CERN: public web. *The Large Hadron Collider*. http://public.web.cern.ch/public/en/lhc/LHCb-en.htm, December 2012.

[3] X. Vidal. *Taking a Closer Look at LHC*. http://www.lhc-closer.es/php/index.php?i=1&s=4&p=9&e=0.

[4] CMS Collaboration. *Compact Muon Solenoid Experiment at CERN's LHC*. http://cms.web.cern.ch, 2008-2012.

[5] SCIENCE in school. *Neutrinos: an introduction*. http://www.scienceinschool.org/print/2274, 2011.

[6] Soler et al. *Large Hadron Collider Phenomenology*. Institute of Physics Publishing, first edition, 2004.

[7] The CMS Collaboration. *The CMS experiment at the CERN LHC*. *JINST*, **3**(08):S08004, 2008.

[8] N. Wermes. *Pixel Vertex Detectors*. *ArXiv Physics e-prints*, November 2006. http://adsabs.harvard.edu/abs/2006physics..11075W.

[9] M. Antonio. *CMSSW Application Framework*. https://twiki.cern.ch/twiki/bin/view/CMSPublic/WorkBookCMSSWFramework.

[10] K. Burkett. *Details of Tracking at CMS*. *Presentation in LHC Physics Workshop (Mumbai)*, October 2009. http://www.ino.tifr.res.in/MaKaC/getFile.py/access?contribId=46&resId=0&materialId=slides&confId=61.

[11] M. Mennea et al. *CMS Tracker Visualisation*. Technical Report CMS-NOTE-2004-009, CERN, Geneva, Jun 2004.

[12] M. Swartz et al. *A new technique for the reconstruction, validation, and simulation of hits in the CMS Pixel Detector*. *PoS*, Vertex 2007(CMS-NOTE-2007-033):035. 37 p, Jul 2007.

[13] A. Dominguez. *CMS Technical Design Report for the Pixel Detector Upgrade*. Technical Report CERN-LHCC-2012-016. CMS-TDR-11, CERN, Geneva, Sep 2012.

[14] C. Lefevre. *LHC: the guide*. https://cds.cern.ch/record/1092437?ln=en, Jan 2008.

[15] B. Martin. *Nuclear and Particle Physics: An Introduction*. John Wiley & Sons, first edition, 2006.

[16] CMS Collaboration. *Observation of a new boson at a mass of 125 GeV with the CMS experiment at the LHC. Phys. Lett. B*, **716**(1):30 – 61, 2012.

[17] ATLAS Collaboration. *Observation of a new particle in the search for the Standard Model Higgs boson with the ATLAS detector at the LHC. Phys. Lett. B*, **716**(1):1 – 29, 2012.

[18] CMS Collaboration. *Search for gluino-mediated bottom- and top-squark production in pp collisions at 8 TeV*. Technical Report CMS-PAS-SUS-12-024, CERN, Geneva, March 2013.

[19] P. Halpern. *Collider: The Search for the World's Smallest Particles*. John Wiley & Sons, first edition, 2009.

[20] I. Dawson. *The SLHC prospects at ATLAS and CMS. J. of Phys.: Conf. Ser.*, **110**(9):092008, 2008.

[21] J. Allday. *Quarks, leptons and the Big Bang*. IoP, second edition, 2002.

[22] B. Povh et al. *Particles and Nuclei: An introduction to the Physical Concepts*. Springer-Verlag, sixth edition, 2008.

[23] J. D. Lykken. *Beyond the Standard Model*. 2010. http://arxiv.org/abs/1005.1676.

[24] CMS Collaboration. *Search for a standard-model-like Higgs boson with a mass of up to 1 TeV at the LHC.* Technical Report arXiv:1304.0213. CMS-HIG-12-034. CERN-PH-EP-2013-050, CERN, Geneva, Mar 2013.

[25] R. Vogt. *Ultrarelativistic Heavy-Ion Collisions.* Elsevier Science, first edition, 2007.

[26] CMS Collaboration. *Technical Proposal for the Upgrade of the CMS detector through 2020.* Technical Report CERN-LHCC-2011-006. LHCC-P-004, CERN, Geneva, Jun 2011.

[27] C. Wong. *Introduction to High-Energy Heavy-Ion Collisions.* World Scientific, first edition, 1994.

[28] C. Genta. *Performances of the CMS Tracker.* Technical Report CMS-CR-2008-098, CERN, Geneva, Nov 2008.

[29] G. Bayatian et al. *CMS Physics: Technical Design Report Volume 1: Detector Performance and Software.* Technical Design Report CMS. CERN, Geneva, 2006.

[30] I. Goitom. *Track Quality Monitoring for The Compact Muon Solenoid Silicon Strip Tracker.* Dissertation, Brunel University, February 2009. http://bura.brunel.ac.uk/handle/2438/3785.

[31] P. Azzurri. *Track Reconstruction Performance in CMS. Nucl. Phys. Proc. Suppl.*, **197**:275–278, December 2009.

[32] G. Cerati. *MultiTrackValidator.* https://twiki.cern.ch/twiki/bin/view/CMSPublic/SWGuideMultiTrackValidator, 2009.

[33] CMS-INFN. *CMS Tracker Visualization Software.* http://webcms.ba.infn.it/cms-software/cms-grid/index.php/CMSTrackerVisualizationSoftware/TrackerMap, 2008.

[34] D. Kotlinski. *Pixel Digitizer in CMSSW.* https://twiki.cern.ch/twiki/bin/view/CMSPublic/SWGuidePixelDigitization, November 2009.

[35] J. Kiefer. *Biological Radiation Effects.* Springer Berlin Heidelberg, 1990.

[36] A. Vasilescu. *The Particle Detector BriefBook*. http://rkb.home.cern.ch/rkb/titleD.html, 1999.

[37] M. Swartz. *CMS pixel simulations. Nucl. Instrum. Methods Phys. Res., A*, **511**:88–91, 2003.